INTERNATIONAL JOURNAL FOR NUMERICAL METHODS IN FLUIDS
Int. J. Numer. Meth. Fluids 0000; **00**:1–38
Published online in Wiley InterScience (www.interscience.wiley.com). DOI: 10.1002/fld

Energy dissipative characteristic schemes for the diffusive Oldroyd-B viscoelastic fluid

Mária Lukáčová - Medvid'ová[1], Hirofumi Notsu[2], Bangwei She[3]*

[1]*Institute of Mathematics, University of Mainz, Staudingerweg 9, 55099 Mainz, Germany*
[2] *Waseda Institute of advanced study, Waseda University, 3-4-1-60-209A, Okubo, Shinjuku-ku, 169-8555 Tokyo, Japan*
[3]*Institute of Mathematics AS CR, Žitná 25, 11567 Praha, Czech Republic*

SUMMARY

In this paper we propose new energy dissipative characteristic numerical methods for the approximation of diffusive Oldroyd-B equations, that are based either on the finite element or finite difference discretization. We prove energy stability of both schemes and illustrate their behaviour on a series of numerical experiments. Using both the diffusive model and the logarithmic transformation of the elastic stress we are able to obtain methods that converge as mesh parameter is refined. Copyright © 0000 John Wiley & Sons, Ltd.

Received . . .

KEY WORDS: characteristic finite element; characteristic finite difference; energy stable; viscoelastic fluids; high Weissenberg; logarithmic transformation

1. INTRODUCTION

In industry, laboratory and everyday life a broad class of materials, such as suspensions, solution of polymers and liquid crystals are categorized as complex fluids. Viscoelasticity is one of the most significant features arose in the complex fluids as they show viscous as well as elastic effects. The mathematical model is given by a system of nonlinear partial differential equations, where two non-dimensional parameters, the Reynolds and Weissenberg numbers, quantify viscous and elastic effects, respectively. It is a well-known fact that numerical simulation of the viscoelastic fluids at high Weissenberg numbers is a very challenging problem. The well-known "High Weissenberg Number Problem" (HWNP) has haunted the mathematicians, computer scientists, and engineers for more than 40 years [9, 22, 24–26, 33, 36, 42–46]. When the Weissenberg number exceeds some limits, numerical solutions computed by any standard methods break down exponentially fast in time. Frustratingly, the mechanism of the instability is still a kind of mistery. Possible reasons

*Correspondence to: Bangwei She. Institute of Mathematics AS CR, Žitná 25, 11567 Praha, Czech Republic.
E-mail:she@math.cas.cz

include purely numerical phenomenon, inadequate physical modelling and can even be caused by singular geometry. The motivation of this paper is to propose a possible way to construct stable and convergent schemes for the problem.

The earlier works in the field of numerical simulation of the Oldroyd-B and related viscoelastic models were realized mostly by using the standard finite difference (FD), finite volume (FV) or finite element (FE) method. Let us mention, for example, contributions by Keunings, Crochet and their cooperators [15, 25, 32] (FE), Wapperom, Keunings and Legat [44] (backward-tracking Lagrangian particle method), Crochet, Davies and Walters [14] (FD-FE scheme), Wapperom and Webster [45], Aboubacar, Matallah and Webster [1], Nadau and Sequeira [33] (hybrid FV-FE scheme), Phillips and Williams [37] (semi-Lagrangian finite volume), Xue, Phan-Thien and Tanner [46] (FV). Without exception, all these methods break down at a moderately high Weissenberg number.

Up to now no approach has been found to solve this problem. Nevertheless, some approaches significantly improved the stability, especially the Logarithm Conformation Representation (LCR) approach proposed by Fattal and Kupfermann [19, 20]. The main idea is to reformulate the constitutive law for the elastic stress tensor by means of the logarithmic transformation of the conformation tensor. In fact, the numerical methods based on polynomials fail to catch the exponential profile of the conformation tensor, but are obviously able to catch its logarithm which is polynomial. This approach has been further implemented by Fattal and Kupfermann [20, 24], Turek et al. [16], Alves et al. [2], Pan and Hao [22, 36], Chen et al. [10]. Similar studies can be found by Balci et al [5], who developed the square-root transformation, Alfonso et al. [3], who applied and summarized the kernel conformation transformation. These transformation methods naturally preserve the positivity of the conformation tensor at the discrete level. Another approach to obtain positivity preserving method is based on the direct discretization of the objective derivative, cf. [28, 29, 42].

In this paper we study the stability of the diffusive Oldroyd-B model for the characteristic based finite element and finite difference schemes in the sense of the free energy [23]. Free energy dissipative schemes based on the characteristic and discontinuous Galerkin method have been studied for the Oldroyd-B system by Boyaval et al. [9]. It has been reported that those methods fail to control the free energy in the cavity test [8]. It should be mentioned that the global existence of weak solution is still open for the Oldroyd-B model. Nevertheless, for the diffusive Oldroyd-B model the regularity [13] and the global existence of weak solution [6] have been presented for two dimension. We would like to point out that the diffusive terms indeed do exist in the physical models. Since the order of the diffusion coefficient is much smaller than the viscosity, e.g. 10^{-9}, they are typically neglected, cf. [7, 17, 39] and references therein.

We will combine the successful LCR approach of Fattal and Kupfermann [19, 20] with the benefits of the diffusive model. Our aim is to show the energy stability of the diffusive model and construct energy dissipative characteristic based schemes that are stable and convergent even for high Weissenberg numbers. The paper is organized as follows. In Section 2 we introduce a diffusive Oldroyd-B type viscoelastic model. Section 3 is devoted to the free energy stability of the model. Two characteristic-based numerical methods are presented in Section 4, the finite element, and the finite difference method. Moreover, we study the free energy stability of the schemes on the discrete level in Section 5. Numerical tests are presented in Section 6.

DOI: 10.1002/fld

2. GOVERNING EQUATIONS

Mathematical model describing the motion of incompressible viscoelastic fluids consists of the mass and momentum conservation laws

$$\rho\left(\frac{\partial \mathbf{u}}{\partial t}+\mathbf{u}\cdot\nabla\mathbf{u}\right)=-\nabla p+\nabla\cdot\mathbf{T}, \tag{1a}$$

$$\nabla\cdot\mathbf{u}=0, \tag{1b}$$

where ρ is the fluid density, $\mathbf{u}$ is the velocity, p is the pressure, the stress tensor $\mathbf{T}$ is a function of the rate of deformation tensor $\mathbf{D}$, where $\mathbf{D}(\mathbf{u})=(\nabla\mathbf{u}+\nabla\mathbf{u}^T)/2$. For the Newtonian fluids the constitutive relationship is a linear constitutive law

$$\mathbf{T}=2\mu_0\mathbf{D},$$

with a constant viscosity $\mu_0>0$. On the other hand, for the viscoelastic Oldroyd-B fluids the constitutive law is nonlinear

$$\mathbf{T}+\lambda\overset{\nabla}{\mathbf{T}}=2\mu_0(\mathbf{D}+\lambda_r\overset{\nabla}{\mathbf{D}}), \tag{1c}$$

where $\lambda,\lambda_r>0$ are relaxation and retardation time, the upper convected derivative is defined as

$$\overset{\nabla}{\mathbf{T}}=\frac{\partial\mathbf{T}}{\partial t}+\mathbf{u}\cdot\nabla\mathbf{T}-\nabla\mathbf{u}\mathbf{T}-\mathbf{T}\nabla\mathbf{u}^T.$$

Now we decompose the stress tensor $\mathbf{T}$ into two parts, which are the purely viscous component $2\mu_0\alpha\mathbf{D}$ with $\alpha=\frac{\lambda_r}{\lambda}$, and the so-called extra stress $\boldsymbol{\tau}$, which contributes to elastic properties,

$$\mathbf{T}=\boldsymbol{\tau}+2\mu_0\alpha\mathbf{D}.$$

According to this decomposition, we can simplify the equation (1c) to its elastic part

$$\lambda\overset{\nabla}{\boldsymbol{\tau}}+\boldsymbol{\tau}=2\mu_0(1-\alpha)D, \tag{2}$$

and rewrite the momentum equation (1a) as

$$\rho\left(\frac{\partial\mathbf{u}}{\partial t}+\mathbf{u}\cdot\nabla\mathbf{u}\right)=-\nabla p+\mu_0\alpha\Delta\mathbf{u}+\nabla\cdot\boldsymbol{\tau}. \tag{3}$$

The system (1b), (2) and (3) is called the Oldroyd-B model for the incompressible viscoelastic fluids.

DOI: 10.1002/fld

Taking into account also diffusive effects in the evolution equation of the elastic stress, we get after non-dimensionalization the following equations

$$Re\left(\frac{\partial \mathbf{u}}{\partial t}+\mathbf{u}\cdot\nabla\mathbf{u}\right)=-\nabla p+\alpha\Delta\mathbf{u}+\frac{\beta}{We}\nabla\cdot(\boldsymbol{\sigma}-\mathbf{I}), \tag{4a}$$

$$\nabla\cdot\mathbf{u}=0, \tag{4b}$$

$$\frac{\partial\boldsymbol{\sigma}}{\partial t}+(\mathbf{u}\cdot\nabla)\boldsymbol{\sigma}-\nabla\mathbf{u}\cdot\boldsymbol{\sigma}-\boldsymbol{\sigma}\cdot(\nabla\mathbf{u})^T=\frac{1}{We}(\mathbf{I}-\boldsymbol{\sigma})+\eta\Delta\boldsymbol{\sigma}, \tag{4c}$$

where $\beta=1-\alpha$, $\eta\geq 0$ is a diffusive parameter. Furthermore, $Re=\frac{\rho UL}{\mu_0}$ and $We=\frac{\lambda U}{L}$ are the reference Reynolds and Weissenberg numbers, respectively. Here U is the reference velocity and L is the reference length. In the non-diffusive case we have $\eta=0$. We consider our system in a bounded domain $\mathcal{T}$ with suitable boundary and initial conditions, e.g. $\mathbf{u}|_{\partial\mathcal{T}}=\mathbf{0}$, $\frac{\partial\boldsymbol{\sigma}}{\partial\mathbf{n}}|_{\partial\mathcal{T}}=\mathbf{0}$, $\mathbf{u}(0)=\mathbf{u}_0$, $\boldsymbol{\sigma}(0)=\boldsymbol{\sigma}_0$, $\mathbf{u}_0$ and $\boldsymbol{\sigma}_0$ are given data. In the paper of Constantin and Kliegl [13] the diffusive Oldroyd-B model has been investigated theoretically and the existence of regular solutions has been proven.

As already pointed out in the previous section the Oldroyd-B model is very challenging particularly in the high Weissenberg limit. To overcome this problem several approaches have been studied in the literature. We should point out that up to now no simulation technique has been found to completely solve this problem and to yield stable and accurate numerical solutions for any Weissenberg number. Nevertheless, some approaches significantly improved and stabilized the numerical simulations. In what follows we describe the LCR approach proposed by Fattal and Kupfermann [19, 20] to reduce the numerical blow up in the case of high We. The main idea of this approach is to replace the conformation tensor by a new variable $\boldsymbol{\psi}(x,t)=\ln\boldsymbol{\sigma}(x,t)$ through eigenvalue computations ($\ln\mathbf{A}=\mathbf{R}\ln\boldsymbol{\Lambda}\mathbf{R}^T$). In the case of $\eta=0$ we arrive at

$$\frac{\partial\boldsymbol{\psi}}{\partial t}+(\mathbf{u}\cdot\nabla)\boldsymbol{\psi}-(\boldsymbol{\Omega}\boldsymbol{\psi}-\boldsymbol{\psi}\boldsymbol{\Omega})-2\mathbf{B}=\frac{1}{We}(e^{-\boldsymbol{\psi}}-\mathbf{I}).$$

Here we have used the following decomposition

$$\nabla\mathbf{u}=\mathbf{B}+\boldsymbol{\Omega}+\mathbf{N}\boldsymbol{\sigma}^{-1}, \tag{5}$$

where $\mathbf{B}$ is symmetric and commutes with the conformation tensor $\boldsymbol{\sigma}$, $\boldsymbol{\Omega}$ is anti-symmetric and $\mathbf{N}\boldsymbol{\sigma}^{-1}$ is an additional dummy part which is also anti-symmetric. Their values can be obtained as follows, cf. [19].

If $\boldsymbol{\sigma}$ is proportional to the unit tensor,

$$\mathbf{B}=\mathbf{D}(\mathbf{u}),\quad \boldsymbol{\Omega}=\mathbf{0},\quad \mathbf{N}=(\nabla\mathbf{u}-\mathbf{D}(\mathbf{u}))\mathrm{tr}\boldsymbol{\sigma}/2. \tag{6}$$

DOI: 10.1002/fld

In general, we get the decomposition in the following way:
Step 1. diagonalizing the conformation tensor,

$$\begin{pmatrix} \lambda_1 & 0 \\ 0 & \lambda_2 \end{pmatrix} = \mathbf{R}^T \boldsymbol{\sigma} \mathbf{R}.$$

Step 2. calculating an intermediate matrix

$$\begin{pmatrix} m_{11} & m_{12} \\ m_{21} & m_{22} \end{pmatrix} = \mathbf{R}^T (\nabla \mathbf{u}) \mathbf{R}.$$

Step 3.

$$\mathbf{N} = R \begin{pmatrix} 0 & n \\ -n & 0 \end{pmatrix} R^T, \ \mathbf{B} = \mathbf{R} \begin{pmatrix} m_{11} & 0 \\ 0 & m_{22} \end{pmatrix} \mathbf{R}^T, \ \boldsymbol{\Omega} = \mathbf{R} \begin{pmatrix} 0 & \omega \\ -\omega & 0 \end{pmatrix} \mathbf{R}^T, \tag{7}$$

where $n = (m_{12} + m_{21})/(\lambda_2^{-1} - \lambda_1^{-1})$, and $\omega = (\lambda_2 m_{12} + \lambda_1 m_{21})/(\lambda_2 - \lambda_1)$.

Analogously as in (4) we propose a new diffusive logarithmic model.

$$Re(\frac{\partial \mathbf{u}}{\partial t} + \mathbf{u} \cdot \nabla \mathbf{u}) = -\nabla p + \alpha \Delta \mathbf{u} + \frac{\beta}{We} \nabla \cdot (e^{\boldsymbol{\psi}} - \mathbf{I}), \tag{8a}$$

$$\nabla \cdot \mathbf{u} = 0, \tag{8b}$$

$$\frac{\partial \boldsymbol{\psi}}{\partial t} + (\mathbf{u} \cdot \nabla)\boldsymbol{\psi} - (\boldsymbol{\Omega}\boldsymbol{\psi} - \boldsymbol{\psi}\boldsymbol{\Omega}) - 2\mathbf{B} = \frac{1}{We}(e^{-\boldsymbol{\psi}} - \mathbf{I}) + \varepsilon \Delta \boldsymbol{\psi}. \tag{8c}$$

where $\varepsilon \geq 0$ is a diffusive parameter.

3. FREE ENERGY OF THE DIFFUSIVE OLDROYD-B MODEL

In this section we introduce a free energy for the viscoelastic models. The free energy consists of the kinetic and elastic energy. Actually, the elastic energy is shown to be the entropy of the polymers in the fluid, cf. [23]. Thus the energy stability we are aiming for is in fact the stability of the free energy with respect to time.

Consider a bounded computational domain $\mathcal{T}$. Then the free energy for the Oldroyd-B model reads

$$F(\mathbf{u}, \boldsymbol{\sigma}) = \frac{Re}{2} \int_{\mathcal{T}} |\mathbf{u}|^2 + \frac{\beta}{2We} \int_{\mathcal{T}} \mathrm{tr}(\boldsymbol{\sigma} - \ln \boldsymbol{\sigma} - \mathbf{I}). \tag{9a}$$

On the other hand for the logarithmic formulation (8), it is given as follows

$$F(\mathbf{u}, e^{\boldsymbol{\psi}}) = \frac{Re}{2} \int_{\mathcal{T}} |\mathbf{u}|^2 + \frac{\beta}{2We} \int_{\mathcal{T}} \mathrm{tr}(e^{\boldsymbol{\psi}} - \boldsymbol{\psi} - \mathbf{I}). \tag{9b}$$

The kinetic term $\frac{1}{2}\int_{\mathcal{T}} |\mathbf{u}|^2$ is always non-negative. As we will show later, see (10b), the entropy $\int_{\mathcal{T}} \mathrm{tr}(\boldsymbol{\sigma} - \ln \boldsymbol{\sigma} - \mathbf{I})$ is also non-negative, provided $\boldsymbol{\sigma}$ is symmetric positive-definite.

DOI: 10.1002/fld

It has been shown by Boyaval et al. [9] that the free energy for the Oldroyd-B model decreases in time. Models obeying this property are called dissipative models. Further, Boyaval et al. constructed energy dissipative numerical schemes, which unfortunately did not converge in the sense of mesh refinement.

The main aim of our paper is to extend their results to the diffusive model (8). First, it holds that the free energy for the diffusive Oldroyd-B model (4) decreases in time exponentially fast to zero, see [41] and Remark 1. In this paper we show that this property is inherited by the diffusive model with the logarithmic transformation.

Before studying the stability of our diffusive viscoelastic models we first summarize some useful preliminaries. The first two lemmas have been used and proven by Boyaval et al. [9].

Lemma 1. ([9]) *Let $\boldsymbol{\sigma}, \boldsymbol{\tau} \in R^{d\times d}$ be two symmetric positive-definite matrices then it holds*

$$tr \ln \boldsymbol{\sigma} = \ln \det \boldsymbol{\sigma}, \tag{10a}$$

$$\boldsymbol{\sigma} - \ln \boldsymbol{\sigma} - \mathbf{I} \text{ is symmetric positive semi-definite and } tr(\boldsymbol{\sigma} - \ln \boldsymbol{\sigma} - \mathbf{I}) \geq 0, \tag{10b}$$

$$\boldsymbol{\sigma} + \boldsymbol{\sigma}^{-1} - 2\mathbf{I} \text{ is symmetric positive semi-definite and } tr(\boldsymbol{\sigma} + \boldsymbol{\sigma}^{-1} - 2\mathbf{I}) \geq 0, \tag{10c}$$

$$tr((\ln \boldsymbol{\tau} - \ln \boldsymbol{\sigma})\boldsymbol{\tau}) \geq tr(\boldsymbol{\tau} - \boldsymbol{\sigma}). \tag{10d}$$

Lemma 2. ([9]) *For any symmetric positive-definite matrix $\boldsymbol{\sigma}(t) \in (C^1([0,T)))^{\frac{d(d+1)}{2}}$ we have for any $t \in [0,T)$, that*

$$(\frac{d}{dt}\boldsymbol{\sigma}) : \boldsymbol{\sigma}^{-1} = tr(\boldsymbol{\sigma}^{-1}\frac{d}{dt}\boldsymbol{\sigma}) = \frac{d}{dt} tr(\ln \boldsymbol{\sigma}), \tag{11a}$$

$$(\frac{d}{dt}\ln \boldsymbol{\sigma}) : \boldsymbol{\sigma} = tr(\boldsymbol{\sigma}\frac{d}{dt}\ln \boldsymbol{\sigma}) = \frac{d}{dt} tr\boldsymbol{\sigma}. \tag{11b}$$

The following lemma will be useful in the evaluation of the diffusive terms in the energy estimate. The proof is stated in the Appendix A.1.

Lemma 3. *Let $\boldsymbol{\sigma}, \boldsymbol{\tau} \in R^{d\times d}$ be symmetric positive-definite matrices, f_1 be an increasing function and f_2 be a decreasing function, then we have*

$$(\boldsymbol{\sigma} - \boldsymbol{\tau}) : (f_1(\boldsymbol{\sigma}) - f_1(\boldsymbol{\tau})) \geq 0, \tag{12a}$$

$$(\boldsymbol{\sigma} - \boldsymbol{\tau}) : (f_2(\boldsymbol{\sigma}) - f_2(\boldsymbol{\tau})) \leq 0, \tag{12b}$$

$$\nabla\boldsymbol{\sigma} : \nabla(\boldsymbol{\sigma}^{-1}) \leq 0, \tag{12c}$$

$$\nabla(\ln \boldsymbol{\sigma}) : \nabla\boldsymbol{\sigma} \geq 0. \tag{12d}$$

Theorem 1. *(energy estimates for the diffusive logarithmic Oldroyd-B model)*
Let $(\mathbf{u}, p, \boldsymbol{\psi})$ be a smooth solution to system (8), supplied with the homogeneous Dirichlet boundary condition for velocity, and with the zero Neumann boundary condition for $\boldsymbol{\psi}$. Further, we assume that initially $e^{\boldsymbol{\psi}}$ is a symmetric positive-definite tensor. The free energy satisfies

$$\frac{d}{dt}F(\mathbf{u}, e^{\boldsymbol{\psi}}) + \alpha\int_{\mathcal{T}}|\nabla\mathbf{u}|^2 + \frac{\beta}{2We^2}\int_{\mathcal{T}} tr(e^{\boldsymbol{\psi}} + e^{-\boldsymbol{\psi}} - \mathbf{I}) \leq 0. \tag{13}$$

Prepared using fldauth.cls
DOI: 10.1002/fld

From this estimate it follows that $F(\mathbf{u}, e^{\boldsymbol{\psi}})$ decreases in time exponentially fast to zero.

Proof

By computing the inner product of the momentum equation and the velocity we get

$$\frac{Re}{2}\frac{d}{dt}\int_{\mathcal{T}}|\mathbf{u}|^2+\alpha\int_{\mathcal{T}}|\nabla\mathbf{u}|^2+\frac{\beta}{We}\int_{\mathcal{T}}\nabla\mathbf{u}:e^{\boldsymbol{\psi}}=0. \tag{14}$$

Multiplying the transport equation for the logarithmic conformation tensor with $e^{\boldsymbol{\psi}}-\mathbf{I}$ implies

$$\frac{d}{dt}\int_{\mathcal{T}}\mathrm{tr}(e^{\boldsymbol{\psi}}-\boldsymbol{\psi})=\int_{\mathcal{T}}(\boldsymbol{\Omega\psi}-\boldsymbol{\psi\Omega}+2\mathbf{B}):(e^{\boldsymbol{\psi}}-\mathbf{I})+\frac{1}{We}\mathrm{tr}(2\mathbf{I}-e^{\boldsymbol{\psi}}-e^{-\boldsymbol{\psi}})+\varepsilon\int_{\mathcal{T}}\Delta\boldsymbol{\psi}:(e^{\boldsymbol{\psi}}-\mathbf{I}). \tag{15}$$

Let us note that

$$\int_{\mathcal{T}}(\boldsymbol{\Omega\psi}-\boldsymbol{\psi\Omega}):(e^{\boldsymbol{\psi}}-\mathbf{I})=\int_{\mathcal{T}}(\boldsymbol{\Omega\psi}-\boldsymbol{\psi\Omega}):e^{\boldsymbol{\psi}}=0$$

and

$$\int_{\mathcal{T}}\mathbf{B}:(e^{\boldsymbol{\psi}}-\mathbf{I})=\int_{\mathcal{T}}\nabla\mathbf{u}:e^{\boldsymbol{\psi}}-\int_{\mathcal{T}}\mathrm{tr}\mathbf{B}=\int_{\mathcal{T}}\nabla\mathbf{u}:e^{\boldsymbol{\psi}}.$$

Using the inequality (12d) of Lemma 3 we get for the diffusive terms

$$\int_{\mathcal{T}}\Delta\boldsymbol{\psi}:(e^{\boldsymbol{\psi}}-\mathbf{I})=-\int_{\mathcal{T}}\nabla\boldsymbol{\psi}:\nabla e^{\boldsymbol{\psi}}\leq 0.$$

Then equation (15) can be written as

$$\frac{d}{dt}\int_{\mathcal{T}}\mathrm{tr}(e^{\boldsymbol{\psi}}-\boldsymbol{\psi})=2\int_{\mathcal{T}}\nabla\mathbf{u}:e^{\boldsymbol{\psi}}+\frac{1}{We}\mathrm{tr}(2\mathbf{I}-e^{\boldsymbol{\psi}}-e^{-\boldsymbol{\psi}})-\varepsilon\int_{\mathcal{T}}\nabla\boldsymbol{\psi}:\nabla e^{\boldsymbol{\psi}}. \tag{16}$$

In order to eliminate the term $\int_{\mathcal{T}}\nabla\mathbf{u}:e^{\boldsymbol{\psi}}$, we compute (14) + $\frac{\beta}{2We}\times$ (16) which yields (13)

$$\begin{aligned}&\frac{d}{dt}\int_{\mathcal{T}}\left(\frac{Re}{2}|\mathbf{u}|^2+\frac{\beta}{2We}\mathrm{tr}(e^{\boldsymbol{\psi}}-\boldsymbol{\psi}-\mathbf{I})\right)+\int_{\mathcal{T}}\left(\alpha|\nabla\mathbf{u}|^2+\frac{\beta}{2We^2}\mathrm{tr}(e^{\boldsymbol{\psi}}+e^{-\boldsymbol{\psi}}-2\mathbf{I})\right)\\&=-\frac{\varepsilon\beta}{2We}\int_{\mathcal{T}}\nabla\boldsymbol{\psi}:\nabla e^{\boldsymbol{\psi}}\leq 0.\end{aligned}$$

By (10c) we have $\mathrm{tr}(e^{\boldsymbol{\psi}}+e^{-\boldsymbol{\psi}}-2\mathbf{I})\geq 0$, thus $F(\mathbf{u}, e^{\boldsymbol{\psi}})$ decreases in time as $\frac{dF}{dt}\leq 0$. It is easy to check that $e^{-\boldsymbol{\psi}}$ is also a symmetric positive-definite matrix. Substituting $e^{-\boldsymbol{\psi}}$ to (10b) yields

$$\mathrm{tr}(e^{-\boldsymbol{\psi}}+\ln(e^{\boldsymbol{\psi}})-\mathbf{I})\geq 0,$$

which implies

$$\mathrm{tr}(e^{\boldsymbol{\psi}}+e^{-\boldsymbol{\psi}}-2\mathbf{I})=\mathrm{tr}(e^{\boldsymbol{\psi}}-\ln e^{\boldsymbol{\psi}}-\mathbf{I})+\mathrm{tr}(e^{-\boldsymbol{\psi}}+\ln(e^{\boldsymbol{\psi}})-\mathbf{I})\geq\mathrm{tr}(e^{\boldsymbol{\psi}}-\ln e^{\boldsymbol{\psi}}-\mathbf{I}).$$

Prepared using fldauth.cls
DOI: 10.1002/fld

Using the Poincaré inequality, we know that there exists a constant $C_p > 0$ depending on the domain $\mathcal{T}$ such that for all $\mathbf{u} \in H_0^1(\mathcal{T})$

$$\int_{\mathcal{T}} |\mathbf{u}|^2 \leq C_p \int_{\mathcal{T}} |\nabla \mathbf{u}|^2.$$

Consequently, we obtain

$$\frac{d}{dt} F(\mathbf{u}, e^{\boldsymbol{\psi}}) \leq -\frac{\alpha}{C_p} \int_{\mathcal{T}} |\mathbf{u}|^2 - \frac{\beta}{2We^2} \mathrm{tr}(e^{\boldsymbol{\psi}} - \ln e^{\boldsymbol{\psi}} - \mathbf{I})) \leq -\min\left(\frac{2\alpha}{Re\, C_p}, \frac{1}{We}\right) F(\mathbf{u}, e^{\boldsymbol{\psi}}).$$

Now we can apply the Gronwall inequality and obtain

$$F(\mathbf{u}, e^{\boldsymbol{\psi}}) \leq F(\mathbf{u}(t=0), e^{\boldsymbol{\psi}}(t=0)) \exp\left(-\min\left(\frac{2\alpha}{Re\, C_p}, \frac{1}{We}\right) t\right),$$

which concludes the proof. □

Remark 1. *The energy inequality also holds for the diffusive Oldroyd-B (4) without LCR technique. Taking the same assumptions as in Theorem 1 the following inequality holds, cf. [41].*

$$F(\mathbf{u}, \boldsymbol{\sigma}) \leq F(\mathbf{u}(t=0), \boldsymbol{\sigma}(t=0)) \exp\left(-\min\left(\frac{2\alpha}{Re\, C_p}, \frac{1}{We}\right) t\right).$$

4. NUMERICAL SCHEMES

In this section we shall present two characteristic type schemes for the diffusive Oldroyd-B model, the characteristic finite element and the characteristic finite difference schemes.

The main idea of the characteristic method is to consider the trajectory of the fluid particle and discretize the material derivative $\frac{D\mathbf{u}}{Dt} = \frac{\partial \mathbf{u}}{\partial t} + \mathbf{u} \cdot \nabla \mathbf{u}$ along the characteristic path defined by the function $\mathbf{X}^n(t, \cdot) : x \in \mathcal{T} \mapsto \mathbf{X}^n(t, x) \in \mathcal{T},\ t \in [t^n, t^{n+1}]$ as

$$\begin{cases} \frac{d}{dt}\mathbf{X}^n(t, \mathbf{x}) = \mathbf{u}_h^n(\mathbf{X}^n(t, \mathbf{x})),\ t \in [t^n, t^{n+1}], \\ \mathbf{X}^n(t^{n+1}, \mathbf{x}) = \mathbf{x}, \end{cases} \tag{17}$$

where $\mathbf{u}_h^n$ is the discrete velocity field. We refer a reader to [34,35,38] for the characteristic schemes applied to the Navier-Stokes equations and to [9] for the non-diffusive Oldroyd-B model. In our real computation, the characteristic position is approximated as

$$\mathbf{X}^n(t^n, \mathbf{x}) \approx \mathbf{x} - u_h^n(\mathbf{x})(t^{n+1} - t^n).$$

4.1. Characteristic FEM

We start with introducing suitable functional spaces and the corresponding weak formulation. Let $\mathcal{T}$ be a bounded domain in $\mathbb{R}^d,\ d = 2, 3$, $V \equiv H_0^1(\mathcal{T})^d$, $Q \equiv L_0^2(\mathcal{T})$ and $W \equiv H^1(\mathcal{T})^{d\times d}$ be the function spaces for the velocity, pressure and conformation tensor. Here $H^1(\mathcal{T})$ and $H_0^1(\mathcal{T})$ are the

DOI: 10.1002/fld

well-known Sobolev spaces, the function space $L_0^2(\mathcal{T})$ is given as

$$L_0^2(\mathcal{T}) \equiv \{q \in L^2(\mathcal{T}); \int_{\mathcal{T}} q dx = 0\}.$$

Further, let $(\cdot,\cdot)$ denote the L^2-inner products in the vector- and matrix- function spaces. In what follows we will use the following bilinear forms

$$a_0(\mathbf{u},\mathbf{v}) = 2\alpha(\mathbf{D}(\mathbf{u}),\mathbf{D}(\mathbf{v})),\ b(\mathbf{u},q) = -(\nabla\cdot\mathbf{u},q),$$
$$\mathcal{A}((\mathbf{u},p),(\mathbf{v},q)) = a_0(\mathbf{u},\mathbf{v}) + b(\mathbf{u},q) + b(\mathbf{v},p).$$

Definition 1. *A weak solution of problem* (8) *is a triple* $\{(\mathbf{u},p,\boldsymbol{\psi})(t)\}_{t\in(0,T)} \subset V\times Q\times W$*, such that for any test function* $(\mathbf{v},q,\boldsymbol{\phi}) \in V\times Q\times W$ *and almost any time* $t\in(0,T)$*, we have*

$$\left(Re\frac{D\mathbf{u}}{Dt}(t),\mathbf{v}\right) + \mathcal{A}((\mathbf{u},p)(t),(\mathbf{v},q)) = \frac{-\beta}{We}(e^{\boldsymbol{\psi}(t)},\nabla\mathbf{v}), \tag{18a}$$

$$\left(\frac{D\boldsymbol{\psi}}{Dt}(t),\boldsymbol{\phi}\right) + \varepsilon(\nabla\boldsymbol{\psi}(t),\nabla\boldsymbol{\phi}) = (\boldsymbol{\Omega}(t)\boldsymbol{\psi}(t) - \boldsymbol{\psi}(t)\boldsymbol{\Omega}(t) + 2\mathbf{B}(t),\boldsymbol{\phi}) + \frac{1}{We}(e^{-\boldsymbol{\psi}(t)} - \mathbf{I},\boldsymbol{\phi}). \tag{18b}$$

Here, $\boldsymbol{\Omega}$ *and* $\mathbf{B}$ *arise from the decomposition* (5)*, and can be derived using equations* (6)*,* (7)*.*

The initial conditions are $\left(\mathbf{u}^0,p^0,\boldsymbol{\sigma}^0(\boldsymbol{\psi}^0=\ln\boldsymbol{\sigma}^0)\right)\in V\times Q\times W$, where $\boldsymbol{\sigma}^0$ is a symmetric positive-definite matrix. In what follows we formulate the characteristic FEM.

As usual, $\mathcal{P}^1(K)$ denotes polynomial space of linear functions on a finite element $K\in\mathcal{T}_h$, $\mathcal{T}_h$ is the triangulation of $\bar{\mathcal{T}}(=\bigcup_{K\in\mathcal{T}_h}K)$, and h_K is the diameter of the element K. We assume that our triangulation is regular, cf. [12].

First, let us define some suitable discrete function spaces $X_h, M_h, \Sigma_h, V_h, Q_h, S_h$ in the following way

$$X_h \equiv \{\mathbf{v}_h\in C^0(\bar{\mathcal{T}}_h)^d; \mathbf{v}_h|_K\in\mathcal{P}^1(K)^d, \forall K\in\mathcal{T}_h\},\ V_h\equiv X_h\cap V,$$
$$M_h \equiv \{q_h\in C^0(\bar{\mathcal{T}}_h); q_h|_K\in\mathcal{P}^1(K), \forall K\in\mathcal{T}_h\},\ Q_h\equiv M_h\cap Q,$$
$$\Sigma_h \equiv \{\boldsymbol{\phi}_h\in C^0(\bar{\mathcal{T}}_h)^{d\times d}; \boldsymbol{\phi}_h|_K\in\mathcal{P}^1(K)^{d\times d}, \forall K\in\mathcal{T}_h\},\ W_h\equiv\Sigma_h\cap W.$$

Further, we introduce some standard interpolation operators [12]

$$\Pi_h^{(1)} : C^0(\bar{\mathcal{T}}_h)^d \to X_h,\quad \Pi_h^{(2)} : C^0(\bar{\mathcal{T}}_h)\to M_h,\quad \Pi_h^{(3)} : C^0(\bar{\mathcal{T}}_h)^{d\times d}\to\Sigma_h.$$

Let Δt denote the time step and N_T the total number of time steps. Now we can formulate our **characteristic FEM** for the diffusive model (8):

DOI: 10.1002/fld

Find $\{(\mathbf{u}_h^{n+1}, p_h^{n+1}, \boldsymbol{\psi}_h^{n+1})\}_{n=0}^{N_T-1} \subset V_h \times Q_h \times W_h$ such that for any test function $(\mathbf{v}_h, q_h, \boldsymbol{\phi}_h) \in V_h \times Q_h \times W_h$ and for $n = 0, \cdots, N_T - 1$, we have

$$\left(Re\frac{\mathbf{u}_h^{n+1} - \mathbf{u}_h^n \circ \mathbf{X}^n(t^n)}{\Delta t}, \mathbf{v}_h\right) + \mathcal{A}((\mathbf{u}_h^{n+1}, p_h^{n+1}), (\mathbf{v}_h, q_h)) + S_h(p_h^{n+1}, q_h) = \frac{-\beta}{We}\left(\Pi_h^{(3)}(e^{\boldsymbol{\psi}_h^{n+1}}), \nabla \mathbf{v}_h\right), \tag{19a}$$

$$\left(\frac{\boldsymbol{\psi}_h^{n+1} - \boldsymbol{\psi}_h^n \circ \mathbf{X}^n(t^n)}{\Delta t}, \boldsymbol{\phi}_h\right) + \varepsilon(\nabla \boldsymbol{\psi}_h^{n+1}, \nabla \boldsymbol{\phi}_h) = (\boldsymbol{\Omega}_h^{n+1}\boldsymbol{\psi}_h^{n+1} - \boldsymbol{\psi}_h^{n+1}\boldsymbol{\Omega}_h^{n+1} + 2\mathbf{B}_h^{n+1}, \boldsymbol{\phi}_h) + \frac{1}{We}\left(\Pi_h^{(3)}(e^{-\boldsymbol{\psi}_h^{n+1}}) - \mathbf{I}, \boldsymbol{\phi}_h\right). \tag{19b}$$

Furthermore, the pressure stabilization term is defined as

$$S_h(p, q) = -\delta \sum_{K \in \mathcal{T}_h} h_K^2 \int_K \nabla p_h \nabla q_h,$$

where $\delta > 0$ is a suitable parameter.

The scheme (19) is implicit in time. In order to obtain a numerical solution for this nonlinear scheme we apply the fixed point iterations. Let us summarize the characteristic FEM (19) in Algorithm 1.

Algorithm 1 Characteristic FEM for the diffusive Oldroyd-B model using the logarithmic transformation

1: Given $\mathbf{u}_h^n, p_h^n, \boldsymbol{\psi}_h^n$, set $\mathbf{u}_h^{n,0} = \mathbf{u}_h^n, \boldsymbol{\psi}_h^{n,0} = \boldsymbol{\psi}_h^n, p_h^{n,0} = p_h^n$.
2: **for** $\ell = 0, 1, \cdots$ **do**
3: solve iteratively the equation (19) with the explicit RHS:

$$\left(Re\frac{\mathbf{u}_h^{n,\ell+1} - \mathbf{u}_h^n \circ \mathbf{X}^n(t^n)}{\Delta t}, \mathbf{v}_h\right) + \mathcal{A}((\mathbf{u}_h^{n,\ell+1}, p_h^{n,\ell+1}), (\mathbf{v}_h, q_h)) + S_h(p_h^{n,\ell+1}, q_h) = \frac{-\beta}{We}\left(\Pi_h^{(3)}(e^{\boldsymbol{\psi}_h^{n,\ell}}), \nabla \mathbf{v}_h\right),$$

$$\left(\frac{\boldsymbol{\psi}_h^{n,\ell+1} - \boldsymbol{\psi}_h^n \circ \mathbf{X}^n(t^n)}{\Delta t}, \boldsymbol{\phi}_h\right) + \varepsilon(\nabla \boldsymbol{\psi}_h^{n,\ell+1}, \nabla \boldsymbol{\phi}_h) = (\boldsymbol{\Omega}_h^{n,\ell}\boldsymbol{\psi}_h^{n,\ell} - \boldsymbol{\psi}_h^{n,\ell}\boldsymbol{\Omega}_h^{n,\ell} + 2\mathbf{B}_h^{n,\ell}, \boldsymbol{\phi}_h) + \frac{1}{We}\left(\Pi_h^{(3)}(e^{-\boldsymbol{\psi}_h^{n,\ell}}) - \mathbf{I}, \boldsymbol{\phi}_h\right).$$

4: **if** $(\|\mathbf{w}^{n,\ell+1} - \mathbf{w}^{n,\ell}\| \le \xi\|\mathbf{w}^{n,\ell}\|$ for $\mathbf{w} \in \{\mathbf{u}_h, p_h, e^{\boldsymbol{\psi}_h}\}$ and ξ is small enough) **then**
5: break
6: **end if**
7: **end for**
8: Update solution: $\mathbf{u}_h^{n+1} = \mathbf{u}_h^{n,\ell+1}, p_h^{n+1} = p_h^{n,\ell+1}, \boldsymbol{\psi}_h^{n+1} = \boldsymbol{\psi}_h^{n,\ell+1}$.

DOI: 10.1002/fld

4.2. *Characteristic finite difference method*

The aim of this section is to present the characteristic finite difference scheme for the diffusive Oldroyd-B model (8) with LCR transformation. In the following, we describe in more details the space and time discretization.

We first discretize the domain $\mathcal{T}_h$ by dividing it into $M \times N$ regular rectangular mesh cells. Let $K_{i,j}$, $i = 1, \cdots, M, j = 1, \cdots, N$, denote an arbitrary cell, h_x be the mesh size in x-direction, and analogously h_y be the mesh size in y-direction. Then the so-called staggered approximation is applied for the fluid flow field. It means that the discretization nodes for velocity components U and V are the midpoints of edges in x- or y-direction, respectively, where $U,\ V$ denote the x and y components of the velocity, cf. Figure 1. Furthermore, nodes for pressure p and logarithm of the conformation tensor $\boldsymbol{\psi}$ are at the cell centers.

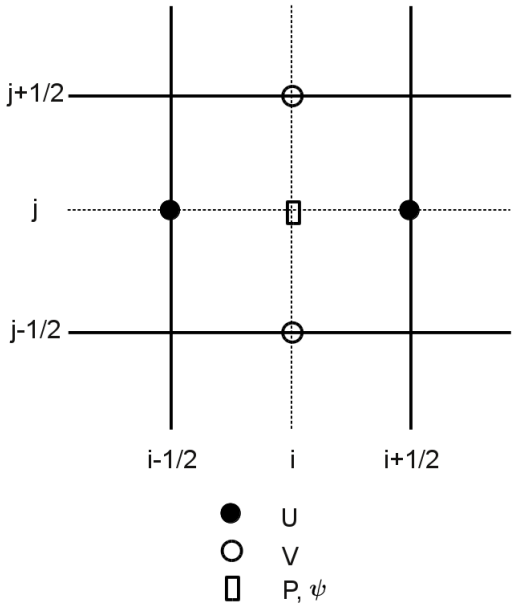

Figure 1. Discretization of the staggered mesh.

In the following, we will split the numerical discretization of the system (8) in two parts. In the first part we apply the characteristic FDM for the transport equation of the logarithmic transformation of the conformation tensor (8c). Specifically, we have

$$\begin{aligned}\frac{\left(\boldsymbol{\psi}^{n+1} - \boldsymbol{\psi}^{n} \circ \mathbf{X}^{n}(t^{n})\right)_{i,j}}{\Delta t} =& (\boldsymbol{\Omega}^{n+1}\boldsymbol{\psi}^{n+1} - \boldsymbol{\psi}^{n+1}\boldsymbol{\Omega}^{n+1} + 2\mathbf{B}^{n+1})_{i,j} \\ &+ \frac{1}{We}(e^{-\boldsymbol{\psi}_{i,j}^{n+1}} - \mathbf{I}) + \varepsilon \Delta_h \boldsymbol{\psi}_{i,j}^{n+1},\end{aligned} \tag{20}$$

where Δt is the time step, $\boldsymbol{\Omega}_{i,j}$ and $\mathbf{B}_{i,j}$ are calculated due to the decomposition (5) of velocity gradient $\nabla_h \mathbf{u}_{i,j}$, see formulas (6), (7). The discrete gradient operator for velocity is defined as

$$\nabla_h \mathbf{u}_{i,j} = \begin{pmatrix} \delta_x U_{i,j} & \delta_y U_{i,j} \\ \delta_x V_{i,j} & \delta_y V_{i,j} \end{pmatrix}, \tag{21a}$$

DOI: 10.1002/fld

where

$$
\begin{aligned}
(\delta_x U)_{i,j} &:= \frac{U_{i+1/2,j} - U_{i-1/2,j}}{h_x},\ (\delta_y V)_{i,j} := \frac{V_{i,j+1/2} - V_{i,j-1/2}}{h_y},\\
(\delta_y U)_{i,j} &:= \frac{U_{i+1/2,j+1} + U_{i-1/2,j+1} - U_{i+1/2,j-1} - U_{i-1/2,j-1}}{4h_y},\\
(\delta_x V)_{i,j} &:= \frac{V_{i+1,j-1/2} + V_{i+1,j+1/2} - V_{i-1,j-1/2} - V_{i-1,j+1/2}}{4h_x}.
\end{aligned}
\tag{21b}
$$

The discrete Laplace operator for $\boldsymbol{\psi}$ is defined as

$$
\Delta_h \boldsymbol{\psi}_{i,j} := \frac{1}{h_x^2}(\boldsymbol{\psi}_{i+1,j} - 2\boldsymbol{\psi}_{i,j} + \boldsymbol{\psi}_{i-1,j}) + \frac{1}{h_y^2}(\boldsymbol{\psi}_{i,j+1} - 2\boldsymbol{\psi}_{i,j} + \boldsymbol{\psi}_{i,j-1}). \tag{22}
$$

In the second part, we apply a suitable FD approximation for the flow equations (8a) and (8b). The idea of this part follows the Chorin projection method, cf. [11,40]. For divergence free functions the convective term $\mathbf{u}\cdot\nabla\mathbf{u}$ is equivalent to $\nabla\cdot(\mathbf{u}\otimes\mathbf{u})$, which is used for the finite difference approximation. The pressure term is treated implicitly in a projection step. More precisely, the FD approximation reads

$$
\begin{aligned}
Re\frac{(U^{n+1}-U^n)_{i+1/2,j}}{\Delta t} =& - Re\delta_x(U^{n+1})^2_{i+1/2,j} - Re\delta_y(U^{n+1}V^{n+1})_{i+1/2,j} - (\delta_x p^{n+1})_{i+1/2,j}\\
&+ \alpha\Delta_h U^{n+1}_{i+1/2,j} + \frac{\beta}{We}(\delta_x\sigma^{n+1}_{11})_{i+1/2,j} + \frac{\beta}{We}(\delta_y\sigma^{n+1}_{12})_{i+1/2,j}, \quad (23a)\\
Re\frac{(V^{n+1}-V^n)_{i,j+1/2}}{\Delta t} =& - Re\delta_x(U^{n+1}V^{n+1})_{i+1/2,j} - Re\delta_y(V^{n+1})^2_{i+1/2,j} - (\delta_y p^{n+1})_{i,j+1/2}\\
&+ \alpha\Delta_h V^{n+1}_{i,j+1/2} + \frac{\beta}{We}(\delta_x\sigma^{n+1}_{21})_{i,j+1/2} + \frac{\beta}{We}(\delta_y\sigma^{n+1}_{22})_{i,j+1/2}, \quad (23b)\\
\nabla_h\cdot\mathbf{u}^{n+1}_{i,j} :=& \delta_x U^{n+1}_{i,j} + \delta_y V^{n+1}_{i,j} = 0. \quad (23c)
\end{aligned}
$$

Here the discrete difference operators for the convective terms are defined as follows

$$
\begin{aligned}
(\delta_x U^2)_{i+1/2,j} &:= \frac{\left((\bar{U}^h)^2 - \gamma|\bar{U}^h|\widetilde{U}^h\right)_{i+1,j} - \left((\bar{U}^h)^2 - \gamma|\bar{U}^h|\widetilde{U}^h\right)_{i,j}}{h_x},\\
(\delta_y(UV))_{i+1/2,j} &:= \frac{(\bar{U}^v\bar{V}^h - \gamma|\bar{V}^h|\widetilde{U}^v)_{i+1/2,j+1/2} - (\bar{U}^v\bar{V}^h - \gamma|\bar{V}^h|\widetilde{U}^v)_{i+1/2,j-1/2}}{h_y},\\
(\delta_x(UV))_{i,j+1/2} &:= \frac{(\bar{U}^v\bar{V}^h - \gamma|\bar{U}^v|\widetilde{V}^h)_{i+1/2,j+1/2} - (\bar{U}^v\bar{V}^h - \gamma|\bar{U}^v|\widetilde{V}^h)_{i-1/2,j+1/2}}{h_x},\\
(\delta_y V^2)_{i,j+1/2} &:= \frac{\left((\bar{V}^v)^2 - \gamma|\bar{V}^v|\widetilde{V}^v\right)_{i,j+1} - \left((\bar{V}^v)^2 - \gamma|\bar{V}^v|\widetilde{V}^v\right)_{i,j}}{h_y},
\end{aligned}
\tag{24}
$$

where $\gamma = \min(1.2\Delta t\cdot\max(\max|U_{i+1/2,j}|,\max|V_{i,j+1/2}|),1)$, the superscripts "$-$" and "$\sim$" represent the average and difference operators, "h" and "v" denote horizontal (x-direction) and

DOI: 10.1002/fld

vertical (y-direction), i.e.

$$\begin{aligned}
(\bar{U}^h)_{i,j} &:= \frac{U_{i-1/2,j}+U_{i+1/2,j}}{2}, \quad (\widetilde{U}^h)_{i,j} := \frac{U_{i+1/2,j}-U_{i-1/2,j}}{2},\\
(\bar{U}^v)_{i+1/2,j+1/2} &:= \frac{U_{i+1/2,j}+U_{i+1/2,j+1}}{2}, \quad (\widetilde{U}^v)_{i+1/2,j+1/2} := \frac{U_{i+1/2,j+1}-U_{i+1/2,j}}{2},\\
(\bar{V}^h)_{i+1/2,j+1/2} &:= \frac{V_{i+1,j+1/2}+V_{i,j+1/2}}{2}, \quad (\widetilde{V}^h)_{i+1/2,j+1/2} := \frac{V_{i+1,j+1/2}-V_{i,j+1/2}}{2},\\
(\bar{V}^v)_{i,j} &:= \frac{V_{i,j+1/2}+V_{i,j-1/2}}{2}, \quad (\widetilde{V}^v)_{i,j} := \frac{V_{i,j+1/2}-V_{i,j-1/2}}{2}.
\end{aligned} \tag{25}$$

The approximation of convective terms reduces to the averaged central difference for $\gamma = 0$, and conservative upwind for $\gamma = 1$.
The Laplace operator Δ_h for the discrete velocity components is given as

$$\Delta_h U_{i+1/2,j} := \delta_x^2 U_{i+1/2,j} + \delta_y^2 U_{i+1/2,j}, \quad \Delta_h V_{i,j+1/2} := \delta_x^2 V_{i,j+1/2} + \delta_y^2 V_{i,j+1/2}, \tag{26}$$

where

$$\begin{aligned}
\delta_x^2 U_{i+1/2,j} &:= \frac{U_{i-1/2,j}-2U_{i+1/2,j}+U_{i+3/2,j}}{h_x^2}, \quad \delta_x^2 V_{i,j+1/2} := \frac{V_{i+1,j+1/2}-2V_{i,j+1/2}+V_{i-1,j+1/2}}{h_x^2},\\
\delta_y^2 U_{i+1/2,j} &:= \frac{U_{i+1/2,j+1}-2U_{i+1/2,j}+U_{i+1/2,j-1}}{h_y^2}, \quad \delta_y^2 V_{i,j+1/2} := \frac{V_{i,j-1/2}-2V_{i,j+1/2}+V_{i,j+3/2}}{h_y^2}.
\end{aligned}$$

The discrete difference operators for the conformation tensor components are defined as follows

$$\begin{aligned}
\delta_x(\sigma_{11})_{i+1/2,j} &:= \frac{(\sigma_{11})_{i+1,j}-(\sigma_{11})_{i,j}}{h_x}, \quad \delta_y(\sigma_{22})_{i,j+1/2} := \frac{(\sigma_{22})_{i,j+1}-(\sigma_{22})_{i,j}}{h_y},\\
\delta_y(\sigma_{12})_{i+1/2,j} &:= \frac{(\sigma_{12})_{i+1,j+1}+(\sigma_{12})_{i,j+1}-(\sigma_{12})_{i+1,j-1}-(\sigma_{12})_{i,j-1}}{4h_y},\\
\delta_x(\sigma_{21})_{i,j+1/2} &:= \frac{(\sigma_{21})_{i+1,j}+(\sigma_{21})_{i+1,j+1}-(\sigma_{21})_{i-1,j}-(\sigma_{21})_{i-1,j+1}}{4h_x}.
\end{aligned} \tag{27}$$

Analogously, the discrete difference operators for the pressure are defined as

$$\delta_x p_{i+1/2,j} := \frac{p_{i+1,j}-p_{i,j}}{h_x}, \quad \delta_y p_{i,j+1/2} := \frac{p_{i,j+1}-p_{i,j}}{h_y}.$$

In order to solve the nonlinear system (20), (23) implicitly in time, we use the fix point iteration approach. Let ℓ represent the iteration step and $\mathbf{u}^{n,\ell}, p^{n,\ell}, \boldsymbol{\psi}^{n,\ell}$ be the solution of the ℓ-th iteration. Starting from $\ell = 0$, we get the solution for the next iteration step $\ell+1$ in the following way:

Step1: Viscoelastic part We first approximate the viscoelastic part (20) in the following steps:
a) Decompose the velocity gradient $\nabla_h \mathbf{u}_{i,j}^{n,\ell}$ to obtain $\boldsymbol{\Omega}_{i,j}^{n,\ell}$ and $\mathbf{B}_{i,j}^{n,\ell}$ according to (6), (7).

DOI: 10.1002/fld

b) Approximate equation (20) in the following manner

$$\begin{aligned}\boldsymbol{\psi}_{i,j}^{n,\ell+1} - \varepsilon\Delta t\Delta_h\boldsymbol{\psi}_{i,j}^{n,\ell+1} =& \boldsymbol{\psi}_{i,j}^{n} \circ \mathbf{X}^n + \Delta t(\boldsymbol{\Omega}_{i,j}^{n,\ell}\boldsymbol{\psi}_{i,j}^{n,\ell} - \boldsymbol{\psi}_{i,j}^{n,\ell}\boldsymbol{\Omega}_{i,j}^{n,\ell} + 2\mathbf{B}_{i,j}^{n,\ell}) \\ &+ \frac{\Delta t}{We}(e^{-\boldsymbol{\psi}_{i,j}^{n,\ell}} - \mathbf{I}).\end{aligned} \tag{28}$$

c) Update the conformation tensor

$$\boldsymbol{\sigma}_{i,j}^{n,\ell+1} = e^{\boldsymbol{\psi}_{i,j}^{n,\ell+1}}. \tag{29}$$

In what follows we present the algorithm that evaluates the foot value $\boldsymbol{\psi}_{i,j}^{n} \circ \mathbf{X}^n$ for the characteristic of a particle. The current position of the particle is

$$\mathbf{x}(i,j) = (x_i, y_j) = \big((i-1/2)h_x,\ (j-1/2)h_y\big).$$

Now we approximate the position of the particle at the previous time step according to the characteristic (17)

$$\mathbf{x}'(i,j) = (x_{i'}, y_{j'}) = \left(x_i - (\bar{U}^h)_{i,j}^n\Delta t,\ y_j - (\bar{V}^v)_{i,j}^n\Delta t\right),$$

where $\bar{U}_{i,j}^h$ and $\bar{V}_{i,j}^v$ are computed using (25).

Let $i' = x_{i'}/h_x + 0.5,\ j' = y_{j'}/h_y + 0.5$ and $i_L = \lfloor i' \rfloor,\ i_R = i_L + 1,\ j_L = \lfloor j' \rfloor,\ j_R = j_L + 1$, where $\lfloor x \rfloor$ returns the largest integer not greater than x. Suppose that $\mathbf{x}'$ is surrounded by the points $\{P_k, k = 1,2,3,4\}$ (see Figure 2), where

$$\mathbf{x}(P_k) = \mathbf{x}(i_{P_k}, j_{P_k}).$$

It is obvious that $i_{P_1} = i_{P_3} = i_L,\quad i_{P_2} = i_{P_4} = i_R,\quad j_{P_1} = j_{P_2} = j_L,\quad j_{P_3} = j_{P_4} = j_R$. We approximate the old time step value at the foot of the characteristic $\mathbf{x}' = (x_{i'}, y_{j'})$ in the following way:

$$\boldsymbol{\psi}_{i,j}^{n} \circ \mathbf{X}^n(t^n) = \sum_{k=1}^{4} w_k \boldsymbol{\psi}^n(P_k),$$

where $w_k = (1 - i_{P_k} + i')(1 - j_{P_k} + j')$ represents the weight of $k-th$ point, see Figure 2.

DOI: 10.1002/fld

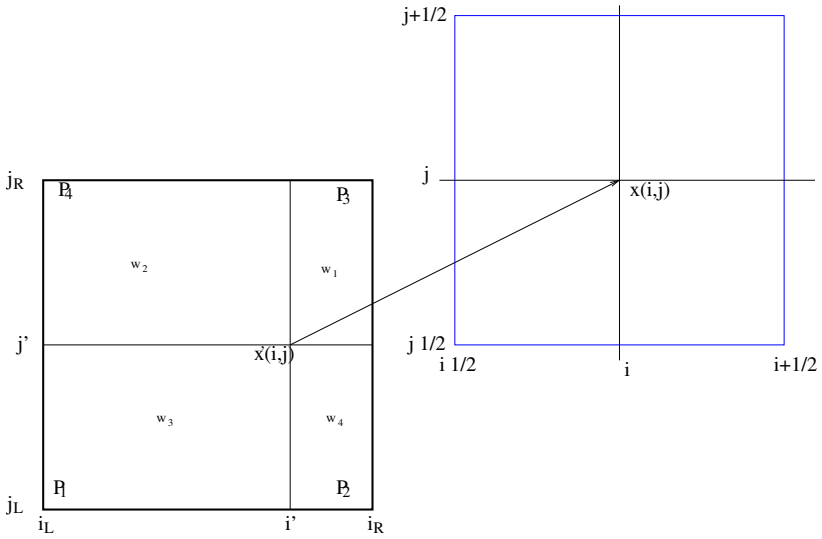

Figure 2. Characteristic position.

Step2: Navier-Stokes part Approximation of the fluid part (23) is realized by the Chorin projection method in two steps.

a) We first neglect the influence of pressure and approximate the following equation

$$Re\mathbf{u}_t - \alpha\Delta\mathbf{u} = -Re\mathbf{u}\cdot\nabla\mathbf{u} + \frac{\beta}{We}\nabla\cdot\boldsymbol{\sigma}.$$

More precisely, it reads

$$\begin{aligned}
\left(\frac{Re}{\Delta t} - \alpha\Delta_h\right) U^*_{i+1/2,j} =& Re\frac{1}{\Delta t}U^n_{i+1/2,j} - Re\delta_x(U^{n,\ell})^2_{i+1/2,j} - Re\delta_y(U^{n,\ell}V^{n,\ell})_{i+1/2,j} \\
&+ \frac{\beta}{We}\left(\delta_x(\sigma_{11}^{n,\ell+1})_{i+1/2,j} + \delta_y(\sigma_{12}^{n,\ell+1})_{i+1/2,j}\right), \\
\left(\frac{Re}{\Delta t} - \alpha\Delta_h\right) V^*_{i,j+1/2} =& Re\frac{1}{\Delta t}V^n_{i,j+1/2} - Re\delta_x(U^{n,\ell}V^{n,\ell})_{i,j+1/2} - Re\delta_y(V^{n,\ell})^2_{i,j+1/2} \\
&+ \frac{\beta}{We}\left(\delta_x(\sigma_{21}^{n,\ell+1})_{i,j+1/2} + \delta_y(\sigma_{22}^{n,\ell+1})_{i,j+1/2}\right).
\end{aligned} \tag{30}$$

b) In the next step we need to approximate the pressure terms $\mathbf{u}_t = \nabla p$, i.e.,

$$\frac{U^{n,\ell+1}_{i+1/2,j} - U^*_{i+1/2,j}}{\Delta t} = -\delta_x p^{n,\ell+1}_{i+1/2,j}, \quad \frac{V^{n,\ell+1}_{i,j+1/2} - V^*_{i,j+1/2}}{\Delta t} = -\delta_y p^{n,\ell+1}_{i,j+1/2}. \tag{31}$$

DOI: 10.1002/fld

This is realized by the following pressure projection step:

b_1) Compute $F_{i,j} = \nabla_h \cdot \mathbf{u}^*_{i,j} \equiv (\delta_x U^*)_{i,j} + (\delta_y V^*)_{i,j}$.

b_2) Solve Poisson equation $-\Delta_h p^{n,\ell+1}_{i,j} = -\dfrac{1}{\Delta t} F_{i,j}$ to get $p^{n,\ell+1}_{i,j}$.

b_3) Update velocity field $\mathbf{u}^{n,\ell+1}_{i,j} = \mathbf{u}^*_{i,j} - \Delta t \nabla_h p^{n,\ell+1}_{i,j}$, i.e.

$U^{n,\ell+1}_{i+1/2,j} = U^*_{i+1/2,j} - \Delta t \delta_x p^{n,\ell+1}_{i+1/2,j}$, and $V^{n,\ell+1}_{i,j+1/2} = V^*_{i,j+1/2} - \Delta t \delta_y p^{n,\ell+1}_{i,j+1/2}$.

Here, the discrete difference operators are defined as follows

$$\nabla_h \cdot \mathbf{u}_{i,j} \coloneqq \delta_x U_{i,j} + \delta_y V_{i,j}, \quad \Delta_h p_{i,j} \coloneqq \delta_x^2 p_{i,j} + \delta_y^2 p_{i,j},$$
$$\delta_x^2 p_{i,j} \coloneqq \frac{p_{i-1,j} - 2p_{i,j} + p_{i+1,j}}{h_x^2}, \quad \delta_y^2 p_{i,j} \coloneqq \frac{p_{i,j-1} - 2p_{i,j} + p_{i,j+1}}{h_y^2},$$

where $\delta_x U_{i,j}$ and $\delta_y V_{i,j}$ are computed using (21).
The incompressibility condition (8b) is naturally satisfied. Indeed, we have

$$\nabla_h \cdot \mathbf{u}^{n,\ell+1}_{i,j} = \nabla_h \cdot \mathbf{u}^*_{i,j} - \Delta t \nabla_h \cdot (\nabla_h p^{n,\ell+1}_{i,j}) = F_{i,j} - \Delta t \Delta_h p^{n,\ell+1}_{i,j} = 0.$$

Finally, we summarize the characteristic FD scheme in the following algorithm

Algorithm 2 Characteristic FD scheme

1: Given $\mathbf{u}^n, p^n, \boldsymbol{\psi}^n$, set $\mathbf{u}^{n,0} = \mathbf{u}^n, \boldsymbol{\psi}^{n,0} = \boldsymbol{\psi}^n, p^{n,0} = p^n$.
2: **for** $\ell = 0, 1, \cdots$ **do**
3: solve the viscoelastic equation (28)
4: update the conformation tensor with equation (29)
5: solve the Navier-Stokes part (30) and (31)
6: **if** ($\|\mathbf{v}^{n,\ell+1} - \mathbf{v}^{n,\ell}\| \le \xi \|\mathbf{v}^{n,\ell}\|$ for $\mathbf{v} \in \{\mathbf{u}, p, \boldsymbol{\sigma}\}$ and ξ is small enough) **then**
7: break
8: **end if**
9: **end for**
10: Update solution: $\mathbf{u}^{n+1} = \mathbf{u}^{n,\ell+1}, p^{n+1} = p^{n,\ell+1}, \boldsymbol{\psi}^{n+1} = \boldsymbol{\psi}^{n,\ell+1}$.

5. ENERGY STABILITY OF THE CHARACTERISTIC SCHEMES

In this section, we shall demonstrate the energy stability of the numerical schemes derived in the previous section.

5.1. Energy stability of the characteristic finite element method, Algorithm 1

In this subsection we will study the diffusive Oldroyd-B model (8), where the logarithmic transformation has been applied for the conformation tensor.

Prepared using fldauth.cls
DOI: 10.1002/fld

Theorem 2. *Let* $(\mathbf{u}_h^n, p_h^n, \boldsymbol{\psi}_h^n)_{0\le n\le N_T}$ *be a solution to* (19) *supplied with homogeneous Dirichlet boundary condition for velocity and with the zero Neumann boundary condition for* $\boldsymbol{\psi}_h$*. Further, we assume that initially* $e^{\boldsymbol{\psi}_h}$ *is a symmetric positive-definite tensor and the determinant of the Jacobi matrix is 1 for any* n*,* $0 \le n \le N_T$*, i.e.*

$$\det\left(\frac{\partial X^n(t^n)}{\partial \mathbf{x}}\right) = 1. \tag{32}$$

Then there exists a $C_k > 0$ *(cf.* (35b)*), such that the free energy of the system* (19)

$$F_h^n = F(\mathbf{u}_h^n, e^{\boldsymbol{\psi}_h^n}) = \frac{Re}{2}\int_{\mathcal{T}_h} |\mathbf{u}_h^n|^2 + \frac{\beta}{2We}\int_{\mathcal{T}_h} tr(e^{\boldsymbol{\psi}_h^n} - \boldsymbol{\psi}_h^n - \mathbf{I})$$

satisfies

$$F_h^{n+1} - F_h^n + \Delta t\int_{\mathcal{T}_h}\left(2\alpha C_k|\nabla \mathbf{u}_h^{n+1}|^2 + \frac{\beta}{2We^2} tr(e^{\boldsymbol{\psi}_h^{n+1}} + e^{-\boldsymbol{\psi}_h^{n+1}} - 2\mathbf{I})\right) \le O(\Delta t h). \tag{33}$$

In particular, the sequence $\{F_h^n\}_{n=0}^{N_T}$ *is non-increasing in the leading order terms having an error of* $O(\Delta t h)$*.*

Proof

We choose $(\mathbf{u}_h^{n+1}, -p_h^{n+1}, \frac{\beta}{2We}(\Pi_h^{(3)}(e^{\boldsymbol{\psi}_h^{n+1}}) - \mathbf{I}))$ as a test function for the system (19) and get

$$\begin{aligned}
0 = &\int_{\mathcal{T}_h}\left(Re\frac{\mathbf{u}_h^{n+1} - \mathbf{u}_h^n\circ X^n(t^n)}{\Delta t}\cdot\mathbf{u}_h^{n+1} + 2\alpha D(\mathbf{u}_h^{n+1}) : D(\mathbf{u}_h^{n+1}) + \frac{\beta}{We}e^{\boldsymbol{\psi}_h^{n+1}} : \nabla\mathbf{u}_h^{n+1}\right)\\
&+ \delta\sum_{K\in\mathcal{T}_h} h_K^2\int_K |\nabla p_h^{n+1}|^2 + \frac{\beta}{2We}\int_{\mathcal{T}_h}\left(\frac{\boldsymbol{\psi}_h^{n+1} - \boldsymbol{\psi}_h^n\circ X^n(t^n)}{\Delta t} : \left(\Pi_h^{(3)}(e^{\boldsymbol{\psi}_h^{n+1}}) - \mathbf{I}\right)\right.\\
&- \left(\boldsymbol{\Omega}_h^{n+1}\boldsymbol{\psi}_h^{n+1} - \boldsymbol{\psi}_h^{n+1}\boldsymbol{\Omega}_h^{n+1} + 2\mathbf{B}_h^{n+1}\right) : \left(\Pi_h^{(3)}(e^{\boldsymbol{\psi}_h^{n+1}}) - \mathbf{I}\right)\\
&\left.- \frac{1}{We}(\mathbf{I} - e^{-\boldsymbol{\psi}_h^{n+1}}) : \left(\Pi_h^{(3)}(e^{\boldsymbol{\psi}_h^{n+1}}) - \mathbf{I}\right) + \varepsilon\nabla\boldsymbol{\psi}_h^{n+1} : \nabla\left(\Pi_h^{(3)}(e^{\boldsymbol{\psi}_h^{n+1}}) - \mathbf{I}\right)\right)\\
\equiv\ & I_1 + I_2 + I_3.
\end{aligned}$$

We separately evaluate $I_1 + I_2$ and I_3, which correspond to the momentum and transport equations, respectively. The assumption (32) implies

$$\int_{\mathcal{T}_h}|\mathbf{u}_h^n\circ X^n(t^n)|^2 = \int_{\mathcal{T}_h}|\mathbf{u}_h^n|^2 \quad\text{and}\quad \int_{\mathcal{T}_h}\boldsymbol{\psi}_h^n\circ X^n(t^n) = \int_{\mathcal{T}_h}\boldsymbol{\psi}_h^n. \tag{34}$$

Prepared using fldauth.cls
DOI: 10.1002/fld

For I_1 and I_2 we have

$$\int_{\mathcal{T}_h} (\mathbf{u}_h^{n+1} - \mathbf{u}_h^n \circ X^n(t^n)) \cdot \mathbf{u}_h^{n+1} = \int_{\mathcal{T}_h} \frac{1}{2}\Big(|\mathbf{u}_h^{n+1}|^2 - |\mathbf{u}_h^n \circ X^n(t^n)|^2 + (\mathbf{u}_h^{n+1} - \mathbf{u}_h^n \circ X^n(t^n))^2\Big)$$
$$\geq \int_{\mathcal{T}_h} \frac{1}{2}\left(|\mathbf{u}_h^{n+1}|^2 - |\mathbf{u}_h^n|^2\right), \tag{35a}$$
$$\int_{\mathcal{T}_h} D(\mathbf{u}_h^{n+1}) : D(\mathbf{u}_h^{n+1}) \geq C_k \int_{\mathcal{T}_h} |\nabla \mathbf{u}_h^{n+1}|^2, \tag{35b}$$
$$I_2 = \delta \sum_{K \in \mathcal{T}_h} h_K^2 \int_K |\nabla p_h^{n+1}|^2 \geq 0, \tag{35c}$$

where the first identity of (34) has been employed for (35a) and C_k in (35b) is a positive constant independent of h and Δt due to the Korn inequality. From (35) we obtain the estimate of the momentum part, $I_1 + I_2$,

$$I_1 + I_2 \geq \frac{Re}{2\Delta t} \int_{\mathcal{T}_h} \left(|\mathbf{u}_h^{n+1}|^2 - |\mathbf{u}_h^n|^2\right) + 2\alpha C_k \int_{\mathcal{T}_h} |\nabla \mathbf{u}_h^{n+1}|^2 + \frac{\beta}{We} \int_{\mathcal{T}_h} e^{\boldsymbol{\psi}_h^{n+1}} : \nabla \mathbf{u}_h^{n+1}. \tag{36}$$

The transport part, I_3, is evaluated as follows. Let $T_i,\ i = 1, \cdots, 5$, be the terms defined by

$$\begin{aligned}
T_1 &\equiv \int_{\mathcal{T}_h} \left(\boldsymbol{\psi}_h^{n+1} - \boldsymbol{\psi}_h^n \circ X^n(t^n)\right) : \left(\Pi_h^{(3)}(e^{\boldsymbol{\psi}_h^{n+1}}) - \mathbf{I}\right) \\
&= \int_{\mathcal{T}_h} \left(\boldsymbol{\psi}_h^{n+1} - \boldsymbol{\psi}_h^n \circ X^n(t^n)\right) : \Pi_h^{(3)}(e^{\boldsymbol{\psi}_h^{n+1}}) - \int_{\mathcal{T}_h} \left(\boldsymbol{\psi}_h^{n+1} - \boldsymbol{\psi}_h^n \circ X^n(t^n)\right) : \mathbf{I} \\
&\equiv T_{11} - T_{12}, \\
T_2 &\equiv \int_{\mathcal{T}_h} (\boldsymbol{\Omega}_h^{n+1}\boldsymbol{\psi}_h^{n+1} - \boldsymbol{\psi}_h^{n+1}\boldsymbol{\Omega}_h^{n+1}) : \left(\Pi_h^{(3)}(e^{\boldsymbol{\psi}_h^{n+1}}) - \mathbf{I}\right), \\
T_3 &\equiv \int_{\mathcal{T}_h} \mathbf{B}_h^{n+1} : \left(\Pi_h^{(3)}(e^{\boldsymbol{\psi}_h^{n+1}}) - \mathbf{I}\right), \qquad T_4 \equiv \int_{\mathcal{T}_h} (\mathbf{I} - e^{-\boldsymbol{\psi}_h^{n+1}}) : \left(\Pi_h^{(3)}(e^{\boldsymbol{\psi}_h^{n+1}}) - \mathbf{I}\right), \\
T_5 &\equiv \int_{\mathcal{T}_h} \nabla \boldsymbol{\psi}_h^{n+1} : \nabla \left(\Pi_h^{(3)}(e^{\boldsymbol{\psi}_h^{n+1}}) - \mathbf{I}\right).
\end{aligned}$$

We know that

$$\begin{aligned}
T_{11} &= \int_{\mathcal{T}_h} (\boldsymbol{\psi}_h^{n+1} - \boldsymbol{\psi}_h^n \circ X^n(t^n)) : \Pi_h^{(3)}(e^{\boldsymbol{\psi}_h^{n+1}}) \\
&= \int_{\mathcal{T}_h} (\boldsymbol{\psi}_h^{n+1} - \boldsymbol{\psi}_h^n \circ X^n(t^n)) : e^{\boldsymbol{\psi}_h^{n+1}} + \int_{\mathcal{T}_h} (\boldsymbol{\psi}_h^{n+1} - \boldsymbol{\psi}_h^n \circ X^n(t^n)) : \left(\Pi_h^{(3)}(e^{\boldsymbol{\psi}_h^{n+1}}) - e^{\boldsymbol{\psi}_h^{n+1}}\right) \\
&= \int_{\mathcal{T}_h} (\boldsymbol{\psi}_h^{n+1} - \boldsymbol{\psi}_h^n \circ X^n(t^n)) : e^{\boldsymbol{\psi}_h^{n+1}} + O(h) \\
&\geq \int_{\mathcal{T}_h} \mathrm{tr}\left(e^{\boldsymbol{\psi}_h^{n+1}} - e^{\boldsymbol{\psi}_h^n \circ X^n(t^n)}\right) + O(h), \\
T_{12} &= \int_{\mathcal{T}_h} \mathrm{tr}(\boldsymbol{\psi}_h^{n+1} - \boldsymbol{\psi}_h^n \circ X^n(t^n)),
\end{aligned}$$

DOI: 10.1002/fld

where we have assumed that our numerical solution is enough regular to obtain $\int_{\mathcal{T}_h} |\Pi_h^{(3)}(e^{\boldsymbol{\psi}_h^{n+1}}) - e^{\boldsymbol{\psi}_h^{n+1}}| = O(h)$. From the fact that $\int_{\mathcal{T}_h} \mathrm{tr}(e^{\boldsymbol{\psi}_h^n} - \boldsymbol{\psi}_h^n) \circ X^n(t^n) = \int_{\mathcal{T}_h} \mathrm{tr}(e^{\boldsymbol{\psi}_h^n} - \boldsymbol{\psi}_h^n)$, cf. (34), we obtain

$$\begin{aligned} T_1 = T_{11} - T_{12} &\geq \int_{\mathcal{T}_h} \mathrm{tr}\Big(\big(e^{\boldsymbol{\psi}_h^{n+1}} - \boldsymbol{\psi}_h^{n+1}\big) - \big(e^{\boldsymbol{\psi}_h^n} - \boldsymbol{\psi}_h^n\big) \circ X^n(t^n) \Big) + O(h) \\ &= \int_{\mathcal{T}_h} \mathrm{tr}\Big(\big(e^{\boldsymbol{\psi}_h^{n+1}} - \boldsymbol{\psi}_h^{n+1}\big) - \big(e^{\boldsymbol{\psi}_h^n} - \boldsymbol{\psi}_h^n\big) \Big) + O(h). \end{aligned} \tag{37}$$

Applying analogous arguments for other terms, we have

$$\begin{aligned} T_2 &= \int_{\mathcal{T}_h} \big(\boldsymbol{\Omega}_h^{n+1}\boldsymbol{\psi}_h^{n+1} - \boldsymbol{\psi}_h^{n+1}\boldsymbol{\Omega}_h^{n+1}\big) : \big(e^{\boldsymbol{\psi}_h^{n+1}} - \mathbf{I}\big) \\ &\quad + \int_{\mathcal{T}_h} \big(\boldsymbol{\Omega}_h^{n+1}\boldsymbol{\psi}_h^{n+1} - \boldsymbol{\psi}_h^{n+1}\boldsymbol{\Omega}_h^{n+1}\big) : \big(\Pi_h^{(3)}(e^{\boldsymbol{\psi}_h^{n+1}}) - e^{\boldsymbol{\psi}_h^{n+1}}\big) \\ &= 0 + O(h), \end{aligned} \tag{38a}$$

$$\begin{aligned} T_3 &= \int_{\mathcal{T}_h} \mathbf{B}_h^{n+1} : \big(e^{\boldsymbol{\psi}_h^{n+1}} - \mathbf{I}\big) + \int_{\mathcal{T}_h} \mathbf{B}_h^{n+1} : \Big(\Pi_h^{(3)}(e^{\boldsymbol{\psi}_h^{n+1}}) - e^{\boldsymbol{\psi}_h^{n+1}}\Big) \\ &= \int_{\mathcal{T}_h} \nabla \mathbf{u}_h^{n+1} : e^{\boldsymbol{\psi}_h^{n+1}} + O(h), \end{aligned} \tag{38b}$$

$$\begin{aligned} T_4 &= \int_{\mathcal{T}_h} \big(\mathbf{I} - e^{-\boldsymbol{\psi}_h^{n+1}}\big) : \big(e^{\boldsymbol{\psi}_h^{n+1}} - \mathbf{I}\big) + \int_{\mathcal{T}_h} \big(\mathbf{I} - e^{-\boldsymbol{\psi}_h^{n+1}}\big) : \Big(\Pi_h^{(3)}(e^{\boldsymbol{\psi}_h^{n+1}}) - e^{\boldsymbol{\psi}_h^{n+1}}\Big) \\ &= \int_{\mathcal{T}_h} \mathrm{tr}\big(e^{\boldsymbol{\psi}_h^{n+1}} + e^{-\boldsymbol{\psi}_h^{n+1}} - 2\mathbf{I}\big) + O(h). \end{aligned} \tag{38c}$$

Note that since $\boldsymbol{\psi}_h^{n+1}$ and $e^{\boldsymbol{\psi}_h^{n+1}}$ commute in (38a), we have

$$\begin{aligned} &\big(\boldsymbol{\Omega}_h^{n+1}\boldsymbol{\psi}_h^{n+1} - \boldsymbol{\psi}_h^{n+1}\boldsymbol{\Omega}_h^{n+1}\big) : \big(e^{\boldsymbol{\psi}_h^{n+1}} - \mathbf{I}\big) = \big(\boldsymbol{\Omega}_h^{n+1}\boldsymbol{\psi}_h^{n+1} - \boldsymbol{\psi}_h^{n+1}\boldsymbol{\Omega}_h^{n+1}\big) : e^{\boldsymbol{\psi}_h^{n+1}} \\ &= \mathrm{tr}\Big(\big(\boldsymbol{\Omega}_h^{n+1}\boldsymbol{\psi}_h^{n+1} - \boldsymbol{\psi}_h^{n+1}\boldsymbol{\Omega}_h^{n+1}\big) e^{\boldsymbol{\psi}_h^{n+1}} \Big) = 0. \end{aligned}$$

Further, the identity $\mathrm{tr}\mathbf{B}_h^{n+1} = \nabla \cdot u_h^{n+1}$ has been employed in (38b). By using the fact that the gradient of piecewise linear function is piecewise constant and the inequality (12d), the viscous term gives

$$\begin{aligned} T_5 &= \int_{\mathcal{T}_h} \nabla \psi_h^{n+1} : \nabla \Big(\Pi_h^{(3)}(e^{\boldsymbol{\psi}_h^{n+1}}) - \mathbf{I}\Big) = \sum_K \int_K \nabla \psi_h^{n+1} : \nabla \Pi_h^{(3)}(e^{\boldsymbol{\psi}_h^{n+1}}) \\ &= \sum_K \int_K \nabla \psi_h^{n+1}(P_i^K) : \nabla e^{\boldsymbol{\psi}_h^{n+1}}(P_i^K) \geq 0, \end{aligned} \tag{39}$$

DOI: 10.1002/fld

where P_i^K is an arbitrary fixed vertex of triangle K. Putting (37), (38) and (39) together, we get the estimate of the transport part, I_3,

$$I_3 \geq \frac{\beta}{2We\Delta t}\int_{\mathcal{T}_h} \mathrm{tr}\Big(\big(e^{\boldsymbol{\psi}_h^{n+1}} - \boldsymbol{\psi}_h^{n+1}\big) - \big(e^{\boldsymbol{\psi}_h^{n}} - \boldsymbol{\psi}_h^{n}\big)\Big) - \frac{\beta}{We}\int_{\mathcal{T}_h} \nabla \mathbf{u}_h^{n+1} : e^{\boldsymbol{\psi}_h^{n+1}} + \frac{\beta}{2We^2}\int_{\mathcal{T}_h} \mathrm{tr}\big(e^{\boldsymbol{\psi}_h^{n+1}} + e^{-\boldsymbol{\psi}_h^{n+1}} - 2\mathbf{I}\big) + O(h). \tag{40}$$

From (36) and (40) we obtain the energy inequality (33), i.e.,

$$F_h^{n+1} - F_h^n \leq -\Delta t \int_{\mathcal{T}_h} \Big(2\alpha C_k |\nabla \mathbf{u}_h^{n+1}|^2 + \frac{\beta}{2We^2}\mathrm{tr}(e^{\boldsymbol{\psi}_h^{n+1}} + e^{-\boldsymbol{\psi}_h^{n+1}} - 2\mathbf{I})\Big) + O(\Delta t h).$$

Thus the free energy inequality implies that we have for leading order terms

$$F_h^{n+1} \leq F_h^n$$

with the error of $O(h^2)$ by assuming that $\Delta t = O(h)$. □

Remark 2. *It should be noted that assuming (32), we actually suppose that the approximation of the discrete velocity field is divergence free* $\nabla \cdot \mathbf{u}_h^n = 0$. *In fact, we have*

$$-\int_{\mathcal{T}_h} \nabla \cdot \mathbf{u}_h^{n+1} q_h - \delta \sum_{K\in\mathcal{T}_h} h_K^2 \int_K \nabla p_h^{n+1} \nabla q_h = 0 \text{ for any } q_h \in Q_h.$$

Taking into account that the second term is small, we have $\nabla \cdot \mathbf{u}_h^{n+1} \approx 0$ *in* $\mathcal{T}_h$.

In the characteristic FD scheme, see Theorem 3 below, we do not need the above assumption as the strong incompressibility condition is naturally satisfied. For our characteristic finite element method an alternative way to obtain the strong incompressibility condition is to use the orthogonal projection, cf. [9, 38].

5.2. *Energy stability of the characteristic finite difference method, Algorithm 2*

In this subsection we will show that the characteristic finite difference scheme also dissipates the free energy. To this end, we introduce some useful discrete integration by parts techniques in Lemma 4–6. We note that the proofs of these Lemmas can be found in [41].

DOI: 10.1002/fld

Lemma 4. ([41]) *For the discrete difference of the transport terms* (24) *appearing in the momentum equation* (23) *the following properties hold*

$$\sum_{i=1}^{M-1}\sum_{j=1}^{N}\left(U\delta_x(U^2)\right)_{i+1/2,j} \geq \frac{1}{4}\sum_{i=1}^{M-1}\sum_{j=1}^{N}(U_{i+1/2,j})^2\Big((\delta_x U)_{i+1,j}+(\delta_x U)_{i,j}\Big), \tag{41a}$$

$$\sum_{i=1}^{M-1}\sum_{j=1}^{N}\left(U\delta_y(UV)\right)_{i+1/2,j} \geq \frac{1}{4}\sum_{i=1}^{M-1}\sum_{j=1}^{N}(U_{i+1/2,j})^2\Big((\delta_y V)_{i,j}+(\delta_y V)_{i+1,j}\Big), \tag{41b}$$

$$\sum_{i=1}^{M}\sum_{j=1}^{N-1}\left(V\delta_x(UV)\right)_{i,j+1/2} \geq \frac{1}{4}\sum_{i=1}^{M}\sum_{j=1}^{N-1}(V_{i,j+1/2})^2\Big((\delta_x U)_{i,j+1}+(\delta_x U)_{i,j}\Big), \tag{41c}$$

$$\sum_{i=1}^{M}\sum_{j=1}^{N-1}\left(V\delta_y(V^2)\right)_{i,j+1/2} \geq \frac{1}{4}\sum_{i=1}^{M}\sum_{j=1}^{N-1}(V_{i,j+1/2})^2\Big((\delta_y V)_{i,j+1}+(\delta_y V)_{i,j}\Big). \tag{41d}$$

The next lemma presents the discrete derivative calculus for the velocity Laplace terms defined in (26).

Lemma 5. ([41]) *Let us define*

$$|\nabla_h U_{i+1/2,j}|^2 := \frac{1}{2}\left((\delta_x U)^2_{i+1,j}+(\delta_x U)^2_{i,j}+(\delta_y U)^2_{i+1/2,j+1/2}+(\delta_y U)^2_{i+1/2,j-1/2}\right),$$
$$|\nabla_h V_{i,j+1/2}|^2 := \frac{1}{2}\left((\delta_x V)^2_{i+1/2,j+1/2}+(\delta_x V)^2_{i-1/2,j+1/2}+(\delta_y V)^2_{i,j+1}+(\delta_y V)^2_{i,j}\right).$$

Then we have the following properties for the Laplace terms used in the momentum equations (23)

$$\sum_{i=1}^{M-1}\sum_{j=1}^{N}(\Delta_h U)_{i+1/2,j}\,U_{i+1/2,j} \leq -\sum_{i=1}^{M-1}\sum_{j=1}^{N}|\nabla_h U_{i+1/2,j}|^2, \tag{42a}$$

$$\sum_{i=1}^{M}\sum_{j=1}^{N-1}(\Delta_h V)_{i,j+1/2}\,V_{i,j+1/2} \leq -\sum_{i=1}^{M}\sum_{j=1}^{N-1}|\nabla_h V_{i,j+1/2}|^2. \tag{42b}$$

Our next goal is to demonstrate the discrete derivative calculus for the elastic stress tensor defined in (27) and the velocity gradient defined in (21).

Lemma 6. ([41]) *Denoting for simplicity* $A=\sigma_{11}, B=\sigma_{12}, C=\sigma_{22}$ *allows us to rewrite* $\boldsymbol{\sigma}$ *on the finite difference cell* $K_{i,j}$ *as*

$$\boldsymbol{\sigma}_{i,j} = \begin{pmatrix} A & B \\ B & C \end{pmatrix}_{i,j}.$$

Let

$$S_1(\boldsymbol{\sigma},\mathbf{u}) := \sum_{i=1}^{M-1}\sum_{j=1}^{N}\left((\delta_x A+\delta_y B)U\right)_{i+1/2,j}+\sum_{i=1}^{M}\sum_{j=1}^{N-1}\left((\delta_x B+\delta_y C)V\right)_{i,j+1/2}, \tag{43a}$$

$$S_2(\boldsymbol{\sigma},\mathbf{u}) := \sum_{i=1}^{M}\sum_{j=1}^{N}(\nabla\mathbf{u}_h:\boldsymbol{\sigma})_{i,j} = \sum_{i=1}^{M}\sum_{j=1}^{N}\left((\delta_x U)A+(\delta_y U)B+(\delta_x V)B+(\delta_y V)C\right)_{i,j}. \tag{43b}$$

DOI: 10.1002/fld

Then the following identity holds

$$S_1(\boldsymbol{\sigma}, \mathbf{u}) + S_2(\boldsymbol{\sigma}, \mathbf{u}) = 0. \tag{44}$$

With the knowledge of above lemmas, we proceed with the main result of this section which demonstrates the dissipation of free energy.

Theorem 3. *Let* $(U^n_{i+1/2,j}, V^n_{i,j+1/2}, p^n_{i,j}, \boldsymbol{\psi}^n_{i,j})_{0\le n\le N_T}$ *be a solution of the discrete characteristic FD scheme, which is the combination of* (23) *and* (20)*, supplied with homogeneous Dirichlet boundary condition for velocity and with the zero Neumann boundary condition for* $\boldsymbol{\psi}_h$*. Further, we assume that initially* $e^{\boldsymbol{\psi}_h}$ *is a symmetric positive-definite tensor. Then the free energy*

$$F^n_h = \frac{Re}{2}\left(\sum_{i=1}^{M-1}\sum_{j=1}^{N}(U^n_{i+1/2,j})^2 + \sum_{i=1}^{M}\sum_{j=1}^{N-1}(V^n_{i,j+1/2})^2\right) + \frac{1-\alpha}{2We}\sum_{i=1}^{M}\sum_{j=1}^{N} tr\left(e^{\boldsymbol{\psi}^n} - \boldsymbol{\psi}^n - \mathbf{I}\right)_{i,j} \tag{45}$$

satisfies

$$\begin{aligned} F^{n+1}_h - F^n_h + \alpha\Delta t\left(\sum_{i=1}^{M-1}\sum_{j=1}^{N}|\nabla_h U^{n+1}_{i+1/2,j}|^2 + \sum_{i=1}^{M}\sum_{j=1}^{N-1}|\nabla_h V^{n+1}_{i,j+1/2}|^2\right) \\ + \frac{\Delta t\beta}{2We^2}\sum_{i=1}^{M}\sum_{j=1}^{N} tr(e^{\boldsymbol{\psi}^{n+1}} + e^{-\boldsymbol{\psi}^{n+1}} - 2\mathbf{I})_{i,j} \le 0. \end{aligned} \tag{46}$$

In particular, the sequence $\{F^n_h\}_{n=0}^{N_T}$ *is non-increasing.*

Proof

Let us first recall the finite difference part of the characteristic FD scheme for the momentum equation, and make the following operations: we multiply (23a) with $U^{n+1}_{i+1/2,j}$, (23b) with $V^{n+1}_{i+1/2,j}$, (23c) with $p^{n+1}_{i,j}$ and sum them together. Let

$$\begin{aligned} S \coloneqq &\sum_{i=1}^{M-1}\sum_{j=1}^{N}\left(Re\frac{(U^{n+1}-U^n)_{i+1/2,j}}{\Delta t} + Re\left(\delta_x(U^{n+1})^2 + \delta_y(UV)^{n+1}\right)_{i+1/2,j}\right)U^{n+1}_{i+1/2,j} \\ &- \left(\alpha(\delta_x^2 U^{n+1} + \delta_y^2 U^{n+1}) - \delta_x p^{n+1} + \frac{\beta}{We}(\delta_x\sigma^{n+1}_{11} + \delta_y\sigma^{n+1}_{12})\right)_{i+1/2,j} U^{n+1}_{i+1/2,j} \\ &+ \sum_{i=1}^{M}\sum_{j=1}^{N-1}\left(Re\frac{(V^{n+1}-V^n)_{i,j+1/2}}{\Delta t} + Re\left(\delta_x(UV)^{n+1} + \delta_y(V^{n+1})^2\right)_{i,j+1/2}\right)V^{n+1}_{i,j+1/2} \\ &- \left(\alpha(\delta_x^2 V^{n+1} + \delta_y^2 V^{n+1}) - \delta_y p^{n+1} + \frac{\beta}{We}(\delta_x\sigma^{n+1}_{21} + \delta_y\sigma^{n+1}_{22})\right)_{i,j+1/2} V^{n+1}_{i,j+1/2} \\ &+ \sum_{i=1}^{M}\sum_{j=1}^{N}\left(\delta_x U^{n+1} + \delta_y V^{n+1}\right)_{i,j} p^{n+1}_{i,j}. \end{aligned} \tag{47}$$

DOI: 10.1002/fld

Obviously, we have $S = 0$. It is easy to get

$$\begin{aligned}(U^{n+1}_{i+1/2,j} - U^{n}_{i+1/2,j}) \cdot U^{n+1}_{i+1/2,j} &= \frac{(U^{n+1}_{i+1/2,j})^2 - (U^{n}_{i+1/2,j})^2}{2} + \frac{(U^{n+1}_{i+1/2,j} - U^{n}_{i+1/2,j})^2}{2} \\ &\geq \frac{(U^{n+1}_{i+1/2,j})^2 - (U^{n}_{i+1/2,j})^2}{2}.\end{aligned} \tag{48}$$

Similarly

$$(V^{n+1}_{i,j+1/2} - V^{n}_{i,j+1/2}) \cdot V^{n+1}_{i,j+1/2} \geq \frac{(V^{n+1}_{i,j+1/2})^2 - (V^{n}_{i,j+1/2})^2}{2}. \tag{49}$$

Using Lemma 4 and the fact that $(\delta_x U + \delta_y V)_{i,j} = 0$ we also obtain

$$\begin{aligned}\sum_{i=1}^{M-1}\sum_{j=1}^{N} \big(U\delta_x(U^2)\big)^{n+1}_{i+1/2,j} + \sum_{i=1}^{M-1}\sum_{j=1}^{N} \big(U\delta_y(UV)\big)^{n+1}_{i+1/2,j} = 0, \\ \sum_{i=1}^{M}\sum_{j=1}^{N-1} \big(V\delta_x(UV)\big)^{n+1}_{i,j+1/2} + \sum_{i=1}^{M}\sum_{j=1}^{N-1} \big(V\delta_y(V^2)\big)^{n+1}_{i,j+1/2} = 0.\end{aligned} \tag{50}$$

For the pressure terms we have

$$\begin{aligned}&\sum_{i=1}^{M-1}\sum_{j=1}^{N} \big((\delta_x p)U\big)^{n+1}_{i+1/2,j} = \frac{1}{h_x}\sum_{j=1}^{N}\sum_{i=1}^{M-1}(p^{n+1}_{i+1,j} - p^{n+1}_{i-1,j})U^{n+1}_{i+1/2,j} \\ &= -\frac{1}{h_x}\sum_{j=1}^{N}\sum_{i=1}^{M}(U^{n+1}_{i+1/2,j} - U^{n+1}_{i-1/2,j})p^{n+1}_{i,j} = -\sum_{i=1}^{M}\sum_{j=1}^{N} \big((\delta_x U)p\big)^{n+1}_{i,j},\end{aligned}$$

and similarly

$$\sum_{i=1}^{M}\sum_{j=1}^{N-1} \big((\delta_y p)V\big)^{n+1}_{i,j+1/2} = -\sum_{i=1}^{M}\sum_{j=1}^{N} \big((\delta_y V)p\big)^{n+1}_{i,j}.$$

Consequently, the following property holds

$$\sum_{i=1}^{M-1}\sum_{j=1}^{N} \big((\delta_x p)U\big)^{n+1}_{i+1/2,j} + \sum_{i=1}^{M}\sum_{j=1}^{N-1} \big((\delta_y p)V\big)^{n+1}_{i,j+1/2} + \sum_{i=1}^{M}\sum_{j=1}^{N} \big((\delta_x U)p + (\delta_y V)p\big)^{n+1}_{i,j} = 0. \tag{51}$$

Using (43a), (48)–(51) and Lemma 5 we derive

$$\begin{aligned}0 = S \geq \frac{-\beta}{We} S_1^{n+1}(\boldsymbol{\sigma}, \mathbf{u}) + \sum_{i=1}^{M-1}\sum_{j=1}^{N} Re\frac{(U^{n+1}_{i+1/2,j})^2 - (U^{n}_{i+1/2,j})^2}{2\Delta t} + \alpha|\nabla_h U^{n+1}_{i+1/2,j}|^2 \\ + \sum_{i=1}^{M}\sum_{j=1}^{N-1} Re\frac{(V^{n+1}_{i,j+1/2})^2 - (V^{n}_{i,j+1/2})^2}{2\Delta t} + \alpha|\nabla_h V^{n+1}_{i,j+1/2}|^2.\end{aligned} \tag{52}$$

DOI: 10.1002/fld

Now we consider the transport equation for the elastic stress tensor $\boldsymbol{\psi}$ and multiply (20) with $(e^{\boldsymbol{\psi}_{i,j}^{n+1}} - \mathbf{I})$. This leads to

$$
\begin{aligned}
0 = S' = &\sum_{i=1}^{M}\sum_{j=1}^{N} \frac{(\boldsymbol{\psi}^{n+1} - \boldsymbol{\psi}^n \circ X^n)_{i,j}}{\Delta t} : (e^{\boldsymbol{\psi}^{n+1}} - \mathbf{I})_{i,j} \\
&- \left(\boldsymbol{\Omega}^{n+1}\boldsymbol{\psi}^{n+1} - \boldsymbol{\psi}^{n+1}\boldsymbol{\Omega}^{n+1} + 2\mathbf{B}^{n+1} + \frac{1}{We}(e^{-\boldsymbol{\psi}^{n+1}} - \mathbf{I}) + \varepsilon\Delta_h\boldsymbol{\psi}^{n+1} \right)_{i,j} : (e^{\boldsymbol{\psi}^{n+1}} - \mathbf{I})_{i,j}.
\end{aligned} \tag{53}
$$

Similar to the proof of Theorem 2 we have

$$
\begin{aligned}
&\sum_{i=1}^{M}\sum_{j=1}^{N}(\boldsymbol{\psi}^{n+1} - \boldsymbol{\psi}^n \circ X^n)_{i,j} : (e^{\boldsymbol{\psi}_{i,j}^{n+1}} - \mathbf{I}) \geq \sum_{i=1}^{M}\sum_{j=1}^{N} \left(\mathrm{tr}(e^{\boldsymbol{\psi}_{i,j}^{n+1}} - \boldsymbol{\psi}_{i,j}^{n+1}) - \mathrm{tr}(e^{\boldsymbol{\psi}_{i,j}^{n}} - \boldsymbol{\psi}_{i,j}^{n}) \right), \\
&\sum_{i=1}^{M}\sum_{j=1}^{N} \left(\boldsymbol{\Omega}^{n+1}\boldsymbol{\psi}^{n+1} - \boldsymbol{\psi}^{n+1}\boldsymbol{\Omega}^{n+1} + 2\mathbf{B}^{n+1} \right) : (e^{\boldsymbol{\psi}_{i,j}^{n+1}} - \mathbf{I}) = \sum_{i=1}^{M}\sum_{j=1}^{N} 2\nabla\mathbf{u}_{i,j}^{n+1} : e^{\boldsymbol{\psi}_{i,j}^{n+1}}, \\
&\sum_{i=1}^{M}\sum_{j=1}^{N}(e^{-\boldsymbol{\psi}_{i,j}^{n+1}} - \mathbf{I}) : (e^{\boldsymbol{\psi}_{i,j}^{n+1}} - \mathbf{I}) = -\sum_{i=1}^{M}\sum_{j=1}^{N} \mathrm{tr}(e^{-\boldsymbol{\psi}_{i,j}^{n+1}} + e^{\boldsymbol{\psi}_{i,j}^{n+1}} - 2\mathbf{I}).
\end{aligned} \tag{54}
$$

For the diffusive terms, we first obtain

$$
\begin{aligned}
&\sum_{i=1}^{M}\sum_{j=1}^{N} \Delta_h\boldsymbol{\psi}_{i,j}^{n+1} : e^{\boldsymbol{\psi}_{i,j}^{n+1}} = -\sum_{i=1}^{M}\sum_{j=1}^{N} \nabla_h\boldsymbol{\psi}_{i,j}^{n+1} : \nabla_h e^{\boldsymbol{\psi}_{i,j}^{n+1}} \\
&= -\sum_{i=1}^{M}\sum_{j=1}^{N} (\boldsymbol{\psi}_{i+1,j}^{n+1} - \boldsymbol{\psi}_{i-1,j}^{n+1}) : (e^{\boldsymbol{\psi}_{i+1,j}^{n+1}} - e^{\boldsymbol{\psi}_{i-1,j}^{n+1}}) \\
&\quad -\sum_{i=1}^{M}\sum_{j=1}^{N} (\boldsymbol{\psi}_{i,j+1}^{n+1} - \boldsymbol{\psi}_{i,j-1}^{n+1}) : (e^{\boldsymbol{\psi}_{i,j+1}^{n+1}} - e^{\boldsymbol{\psi}_{i,j-1}^{n+1}}) \leq 0,
\end{aligned} \tag{55}
$$

where we have used (12a). Further, it is easy to show

$$
\begin{aligned}
&\sum_{i=1}^{M}\sum_{j=1}^{N} \Delta\boldsymbol{\psi}_{i,j}^{n+1} : \mathbf{I} = \sum_{i=1}^{M}\sum_{j=1}^{N} \mathrm{tr}(\boldsymbol{\psi}_{i+1,j} + \boldsymbol{\psi}_{i,j+1} - 4\boldsymbol{\psi}_{i,j} + \boldsymbol{\psi}_{i-1,j} + \boldsymbol{\psi}_{i,j-1})^{n+1} \\
&= \sum_{i=1}^{M} \mathrm{tr}(\boldsymbol{\psi}_{i,N+1} - \boldsymbol{\psi}_{i,N} - \boldsymbol{\psi}_{i,1} + \boldsymbol{\psi}_{i,0})^{n+1} + \sum_{j=1}^{N} \mathrm{tr}(\boldsymbol{\psi}_{M+1,j} - \boldsymbol{\psi}_{M,j} - \boldsymbol{\psi}_{1,j}\boldsymbol{\psi}_{0,j})^{n+1} \\
&= 0,
\end{aligned} \tag{56}
$$

DOI: 10.1002/fld

due to the corresponding boundary condition.
Combining (54), (55), (56) together yields

$$0 = S' \geq -2S_2^{n+1}(\boldsymbol{\sigma}, \mathbf{u}) + \sum_{i=1}^{M}\sum_{j=1}^{N} \frac{1}{\Delta t}\mathrm{tr}\left((e^{\boldsymbol{\psi}_{i,j}^{n+1}} - \boldsymbol{\psi}_{i,j}^{n+1}) - (e^{\boldsymbol{\psi}_{i,j}^{n}} - \boldsymbol{\psi}_{i,j}^{n})\right) + \mathrm{tr}(e^{\boldsymbol{\psi}_{i,j}^{n+1}} + e^{-\boldsymbol{\psi}_{i,j}^{n+1}} - 2\mathbf{I}). \quad (57)$$

Multiplying (57) with a factor $\frac{\beta}{2We}$, summing with (52) and using (44) together with Lemma 6 leads to

$$\begin{aligned}
&\sum_{i=1}^{M-1}\sum_{j=1}^{N} Re\frac{(U_{i+1/2,j}^{n+1})^2 - (U_{i+1/2,j}^{n})^2}{2\Delta t} + \alpha|\nabla_h U_{i+1/2,j}^{n+1}|^2 \\
&+ \sum_{i=1}^{M}\sum_{j=1}^{N-1} Re\frac{(V_{i,j+1/2}^{n+1})^2 - (V_{i,j+1/2}^{n})^2}{2\Delta t} + \alpha|\nabla_h V_{i,j+1/2}^{n+1}|^2 \\
&+ \sum_{i=1}^{M}\sum_{j=1}^{N} \frac{1}{\Delta t}\frac{\beta}{We}\mathrm{tr}\left((e^{\boldsymbol{\psi}^{n+1}} - \boldsymbol{\psi}^{n+1}) - (e^{\boldsymbol{\psi}^{n}} - \boldsymbol{\psi}^{n})\right)_{i,j} + \frac{\beta}{2We^2}\mathrm{tr}(e^{\boldsymbol{\psi}^{n+1}} + e^{-\boldsymbol{\psi}^{n+1}} - 2\mathbf{I})_{i,j} \\
&\leq 0.
\end{aligned} \quad (58)$$

Consequently, the sequence $\{F_h^n\}_{n=0}^{N_T}$ is non-increasing since we have

$$\begin{aligned}
F^{n+1} - F^n \leq -\Delta t\Bigg(&\alpha\Big(\sum_{i=1}^{M-1}\sum_{j=1}^{N}|\nabla_h U_{i+1/2,j}^{n+1}|^2 + \sum_{i=1}^{M}\sum_{j=1}^{N-1}|\nabla_h V_{i,j+1/2}^{n+1}|^2\Big) \\
&+ \frac{\beta}{2We^2}\sum_{i=1}^{M}\sum_{j=1}^{N}\mathrm{tr}(e^{\boldsymbol{\psi}^{n+1}} + e^{-\boldsymbol{\psi}^{n+1}} - 2\mathbf{I})_{i,j}\Bigg) \leq 0.
\end{aligned} \quad (59)$$

□

Using the discrete integration by parts formulas from the previous subsection we have shown that the characteristic FD method also dissipates the free energy.

Remark 3. *In the case that the characteristic approach is also used to approximate the convective term in the Navier-Stokes part, the energy stability can be proven in an analogous way. Indeed, the only difference to the proof of Theorem 3 is that instead of* (48)–(50) *we have an analogous estimate as in* (35a)

$$\begin{aligned}
\sum_{i=1}^{M-1}\sum_{j=1}^{N}\left(U_{i+1/2,j}^{n+1} - U_{i+1/2,j}^{n}\circ\mathbf{X}^n\right)U_{i+1/2,j}^{n+1} &\geq \sum_{i=1}^{M-1}\sum_{j=1}^{N}\frac{|U_{i+1/2,j}^{n+1}|^2 - |U_{i+1/2,j}^{n}|^2}{2}, \\
\sum_{i=1}^{M}\sum_{j=1}^{N-1}\left(V_{i,j+1/2}^{n+1} - V_{i,j+1/2}^{n}\circ\mathbf{X}^n\right)V_{i,j+1/2}^{n+1} &\geq \sum_{i=1}^{M}\sum_{j=1}^{N-1}\frac{|V_{i,j+1/2}^{n+1}|^2 - |V_{i,j+1/2}^{n}|^2}{2}.
\end{aligned} \quad (60)$$

DOI: 10.1002/fld

6. NUMERICAL TESTS

In this section we illustrate the behaviour of our characteristic schemes and support our theoretical results. In particular our aim is to study the influence of the diffusive parameter ε and the Weissenberg number We on the stability and accuracy of our schemes.

6.1. Lid-driven Cavity

Our first test case is the lid-driven cavity problem. The geometry and mesh of the problem are given in Figure 3.

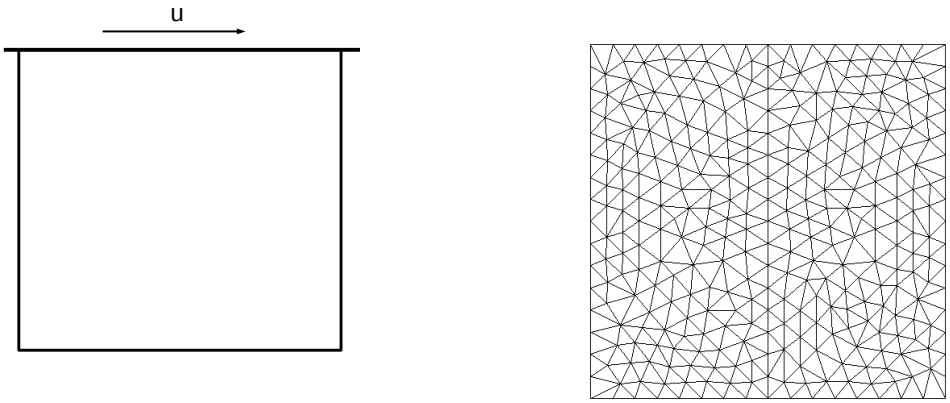

Figure 3. Geometry and mesh for the cavity flow problem.

The computational domain is $\mathcal{T} = [0,1]^2$. The initial conditions are taken to be

$$\mathbf{u} = \mathbf{0}, \quad \boldsymbol{\sigma} = \mathbf{I}. \tag{61}$$

A Dirichlet boundary condition is set for velocity

$$\mathbf{u} = \begin{cases} (16x^2(1-x)^2, 0)^T, & \text{if } y = 1, x \in [0,1], \\ \mathbf{0}, & \text{else.} \end{cases} \tag{62}$$

Further, we choose extrapolated boundary condition for the logarithmic conformation tensor, which means

$$\frac{\partial \boldsymbol{\psi}}{\partial \mathbf{n}} = 0, \tag{63}$$

where $\mathbf{n}$ is the outer normal of the boundary.

Prepared using fldauth.cls
DOI: 10.1002/fld

Influence of the Weissenberg number and the diffusion coefficient ε This subsection aims to study the effects of the Weissenberg number We and the diffusion coefficient ε in the diffusive Oldroyd-B model (8) using the logarithmic transformation. This test is based on the characteristic finite element scheme, Algorithm 1. We fix either the Weissenberg number We and vary the diffusion coefficient ε, or in the opposite way we fix ε and vary We. The free energy is presented in Figures 4 and 5 for Weissenberg numbers $We = 0.1,\ 0.5,\ 1,\ 5,\ 50$ and diffusion coefficients $\varepsilon = 1,\ 1e-1,\ 1e-2,\ 1e-3$. From the two sets of results we can clearly see that the free energy is controlled even for high Weissenberg number. We also note, that for smaller We the free energy converges very fast, while for higher We longer time is required to reach to a steady state.

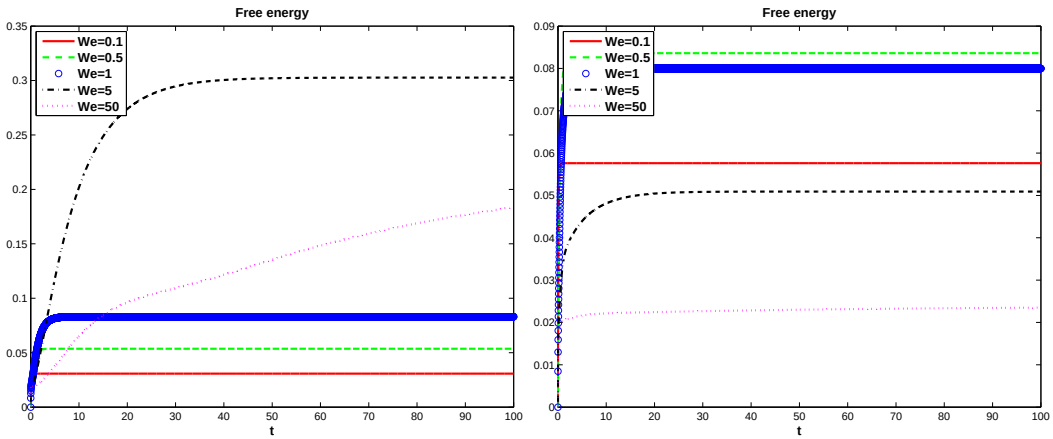

(a) $\varepsilon = 1$

(b) $\varepsilon = 0.1$

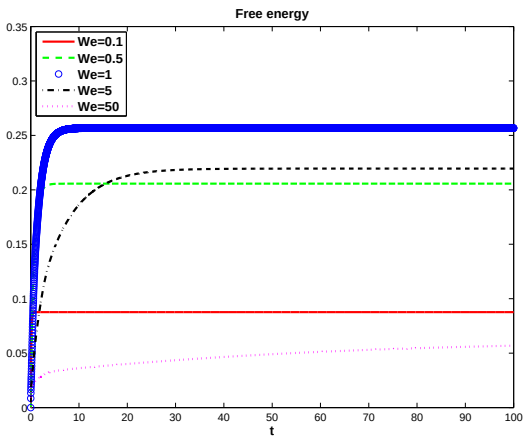

(c) $\varepsilon = 0.01$

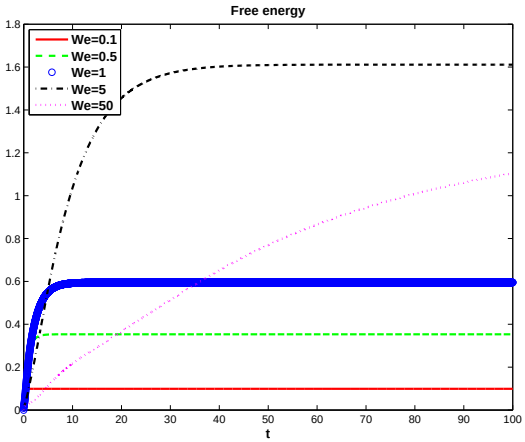

(d) $\varepsilon = 0.001$

Figure 4. Free energy of the diffusive Oldroyd-B model (8) for different We, computed by the characteristic FEM, Algorithm 1.

DOI: 10.1002/fld

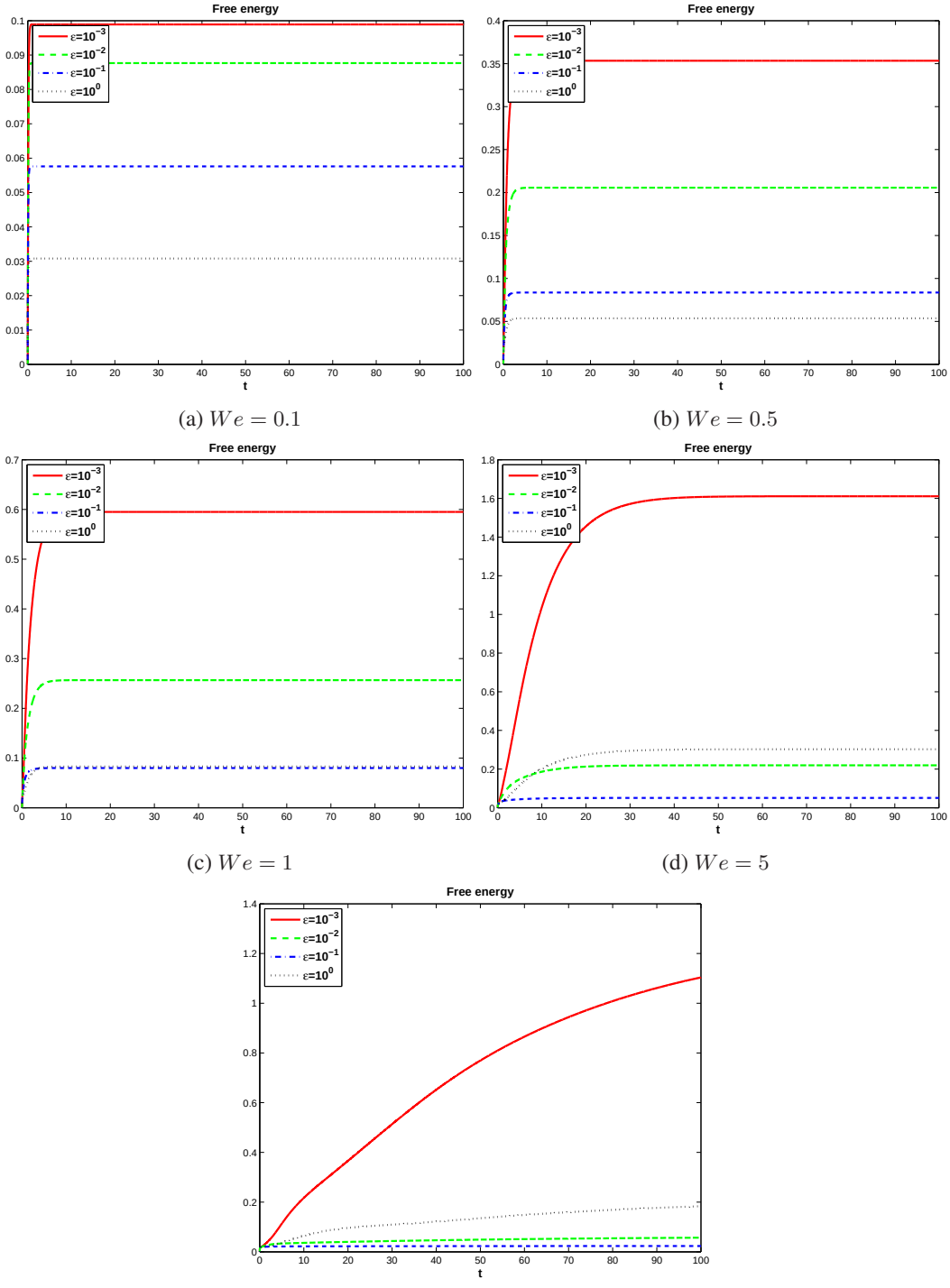

(a) $We = 0.1$ (b) $We = 0.5$

(c) $We = 1$ (d) $We = 5$

(e) $We = 50$

Figure 5. Free energy of the diffusive Oldroyd-B model (8) for different diffusion coefficients ε at $We = 0.5,\ 5$, computed by the characteristic FEM, Algorithm 1.

Analysis of the experimental order of convergence The aim of this section is to analyze the experimental order of convergence of our characteristic schemes for various Weissenberg numbers.

DOI: 10.1002/fld

Let ϕ_h denote the numerical solution and ϕ be the corresponding exact solution. We denote the L^2-error as $e(\phi_h) = \|\phi_h - \phi\|_{L^2}$ and H^1-error $e_1(\phi_h) = \|\phi_h - \phi\|_{H^1}$. In our experiments the exact solution ϕ is replaced by the reference solution computed at a very fine mesh since the exact analytical solution is not available. The experimental order of convergence (EOC) is defined as

$$\text{EOC} = \log_2 \frac{\text{error of } \phi_h}{\text{error of } \phi_{h/2}}.$$

Table I illustrates the mesh convergence results of the characteristic FEM at $t = 30$ for different Weissenberg numbers. The results demonstrate that the EOC is not influenced by the Weissenberg numbers even for relatively small diffusion parameter. Indeed, we have the second order convergence in the L^2-norm for velocity and superlinear convergence for conformation tensor. Besides, we observe the first order convergence for the L^2-norm of pressure and H^1-norm of velocity and stress tensor.

Table II presents the mesh convergence results for the characteristic FDM at $t = 30$ for different Weissenberg numbers. It indicates that the EOC results are similar to those for the characteristic FEM. Interestingly, if the characteristic approximation is applied to both convective terms in the equation of ψ as well as for $\mathbf{u}$, we have obtained a super convergence of the L^2-norm for pressure as well as H^1-norm for velocity, cf. [30, 31]. We present in Table III only the results for $We = 0.5$, the results for other We numbers are analogous.

6.2. 4 to 1 contraction flow

In this test we will consider a well-known benchmark for the viscoelastic fluids, the so-called 4:1 contraction problem. Hereby, the Algorithm 1 will be studied for the diffusive Oldroyd-B model (8). Previous studies on the numerical simulation of this problem can be found, e.g. [1, 4, 18, 33]. One of the main difficulties is the singularity at the re-entrant corner due to the abrupt contraction [21, 33].

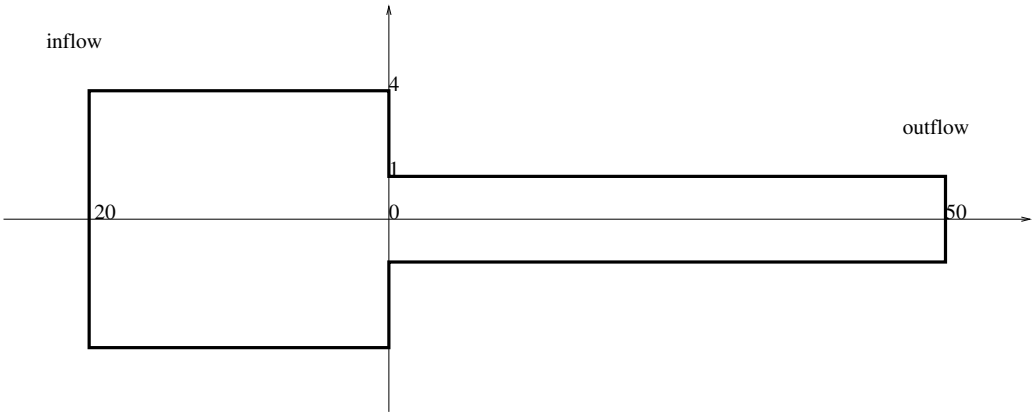

Figure 6. Geometry of 4:1 contraction flow.

As shown in Figure 6, the computational domain is taken to be from -20 to 50 in the x-direction. The upstream has a width of 8 while downstream width is set to be 2. Analogously as in [10, 33] we use only the upper half of the computational domain as it is symmetric with respect to x axis.

DOI: 10.1002/fld

For the velocity we prescribe the parabolic Dirichlet condition on inlet

$$U = \frac{1}{8}\left(1 - y^2/16\right), \; V = 0 \text{ with } \mathbf{u} = (U, V). \tag{64a}$$

At the outflow the zero-Neumann boundary conditions are applied

$$\frac{\partial \mathbf{u}}{\partial \mathbf{n}} = 0.$$

Boundary conditions for the conformation tensor are used as in (63). Moreover, no-slip conditions $U = 0 = V$ are imposed on the solid walls and symmetry conditions are specified on the symmetric axis

$$\sigma_{12}(x, 0) = V(x, 0) = 0. \tag{64b}$$

Other parameters are chosen similarly as in [10, 33], i.e.

$$\alpha = 1/9, Re = 0.$$

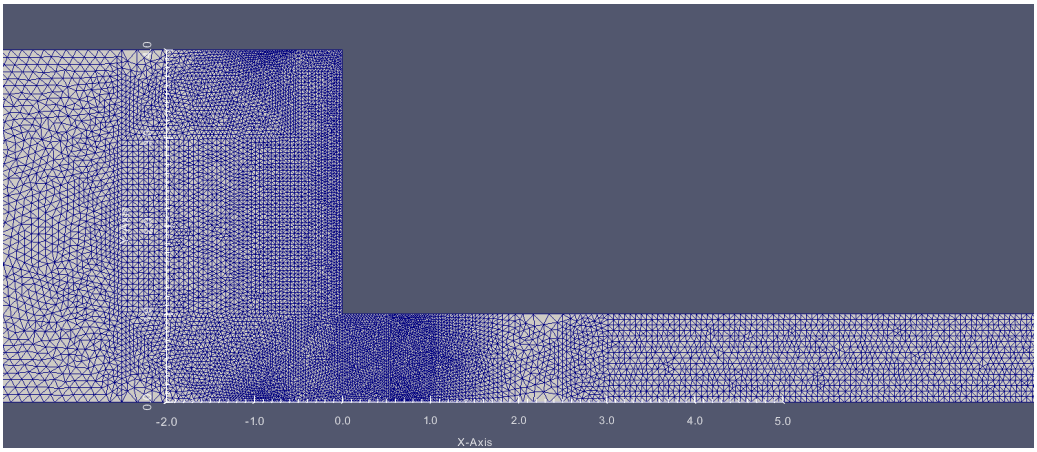

Figure 7. Mesh of 4:1 contraction flow, created by "FreeFEM++-cs" [27].

The center part of the computational mesh for the 4:1 contraction flow together with a local refinement near the abrupt contraction corner is shown in Figure 7. Details of the mesh are as follows. Total number of mesh points and mesh elements are $np = 26538$ and $ne = 50874$, respectively. Maximum, minimum and mean values of the mesh length are $(hmax, hmin, hmean) = (2.05e-01, 1.62e-02, 7.29e-02)$.

6.2.1. Non-diffusive case We first present the results for the non-diffusive case with $\varepsilon = 0$. Figure 8 shows the streamline, pressure and elastic stress tensor for the case $We = 3$ at $t = 1$. We can clearly recognize a big vertex at the corner of abrupt contraction. The pressure is decreasing along the x axis.

In Figure 9 we compare the results for different Weissenberg numbers. Figure 9(a) indicates that the pressure is decreasing along the x axis having a gradual decline rate in the upstream region and

DOI: 10.1002/fld

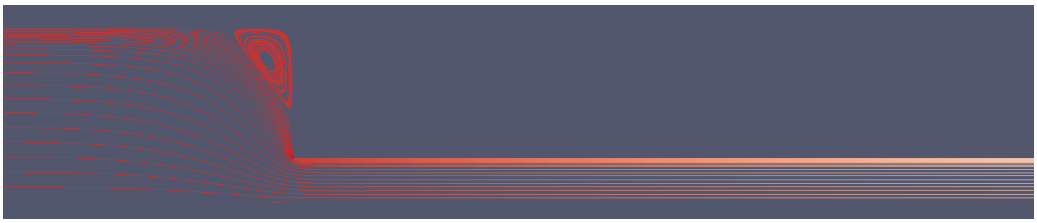

(a) Streamlines

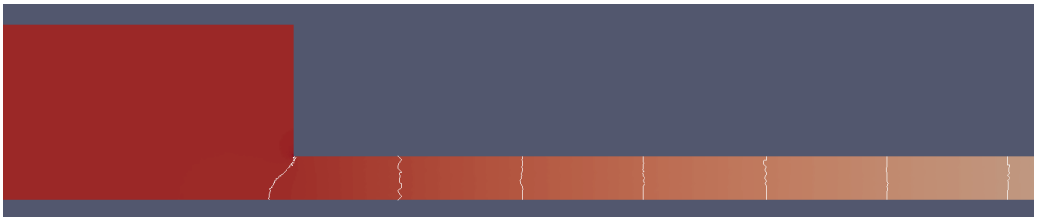

(b) Pressure: min=0, max=19.2

(c) Conformation tensor σ_{11}: min=0.398, max=4.54

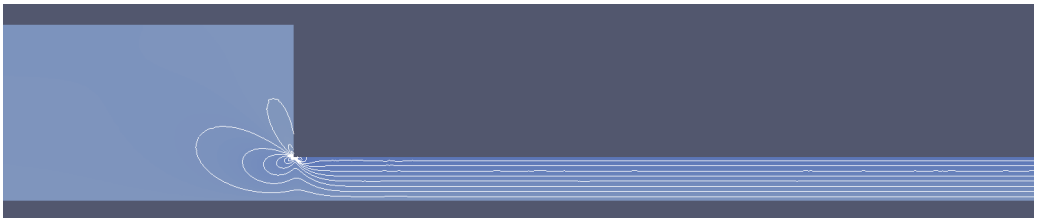

(d) Conformation tensor σ_{12}: min=-2.05, max=0.8

(e) Conformation tensor σ_{22}: min=0.745, max=2.76

Figure 8. Results of the non-diffusive Oldroyd-B model at $We = 3$, $t = 1$, streamlines, pressure isolines, σ_{11}, σ_{12} and σ_{22} isolines, computed by the characteristic FEM, Algorithm 1.

a steeper rate in the downstream channel. Moreover, it can be concluded that larger We number causes to smaller pressure drop at outlet with respect to the inlet pressure. Velocities for different We numbers are almost indistinguishable. In Figures 9(c) and 9(d) we can recognize that jumps of the conformation tensor at the contraction corner increase for larger We.

DOI: 10.1002/fld

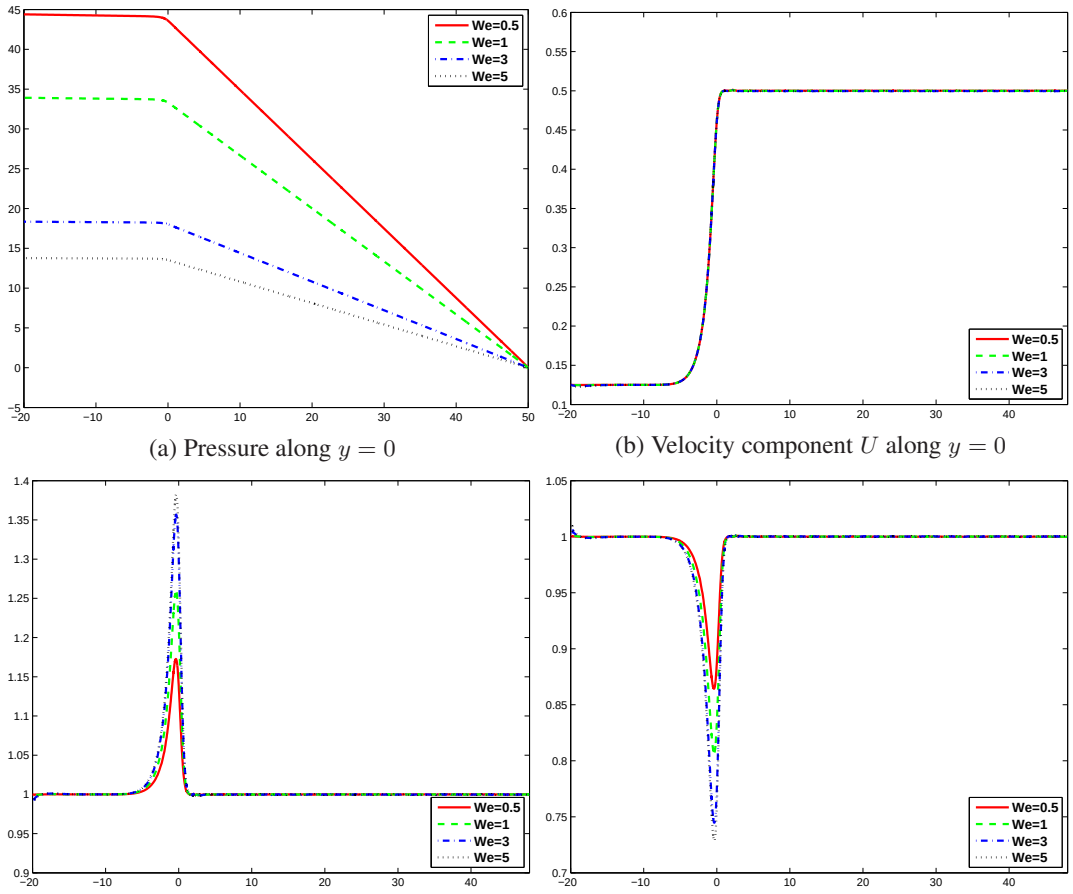

(a) Pressure along $y = 0$

(b) Velocity component U along $y = 0$

(c) σ_{11} along $y = 0$

(d) σ_{22} along $y = 0$

Figure 9. Results of the non-diffusive Oldroyd-B model at $t = 1$ along the symmetric axis $y = 0$ for different We: pressure p, velocity component U, components of the conformation tensor σ_{11} and σ_{22}, computed by the characteristic FEM, Algorithm 1.

6.2.2. Diffusive case In the following test we will present the results for the diffusive case with $\varepsilon > 0$. In Figures 10 and 11 we present the results for fixed diffusive coefficients $\varepsilon = 0.01$ or $\varepsilon = 1$ and different We numbers.

Similar to the non-diffusive model, the pressure is decreasing along x-axis and larger We numbers cause a smaller pressure drop. The jumps of the conformation tensor around the contraction corner increase for larger We numbers. Comparing the results with a small diffusion coefficient, e.g. $\varepsilon \leq 0.01$, the results for larger diffusion ($\varepsilon \geq 1$) are quite different. First, the value of pressure at the inlet decrease for larger ε. Secondly, the velocity in the downstream region along the x-axis increases for larger We numbers, which almost does not change for small diffusion coefficients $\varepsilon \leq 0.01$, see Figures 10(b) and 11(b). The conformation tensor in the downstream region is also changing for different We numbers, e.g. the σ_{22} component of conformation tensor decreases for larger We numbers.

In Figure 12 we show the results of kinetic energy and free energy for different We numbers. We can clearly see, that the kinetic energy does not increase for larger We, while the entropy is increasing quite quickly.

DOI: 10.1002/fld

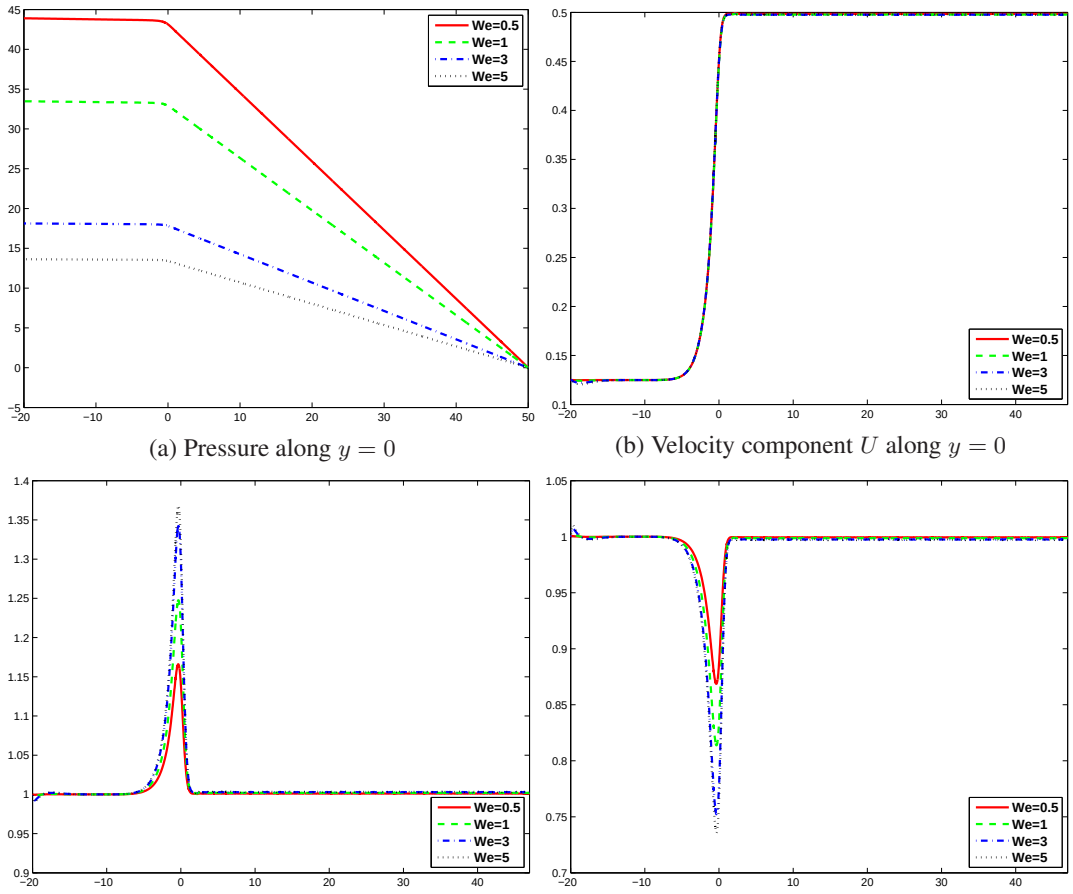

(a) Pressure along $y = 0$

(b) Velocity component U along $y = 0$

(c) σ_{11} along $y = 0$

(d) σ_{22} along $y = 0$

Figure 10. Results of the diffusive Oldroyd-B model, $\varepsilon = 0.01$, at $t = 1$ along the symmetric axis $y = 0$ for different We: pressure p, velocity component U, components of the conformation tensor σ_{11} and σ_{22}, computed by the characteristic FEM, Algorithm 1.

6.3. Discussion

Our numerical experiments demonstrate that the diffusive model is more numerically stable than the non-diffusive one. In the driven cavity test we have obtained the mesh convergent results of the diffusive Oldroyd-B model even for very high Weissenberg numbers, where the logarithmic transformation has been applied. The most important ingredients of the energy stable schemes were approximation of the convective term using the characteristics and the logarithmic transformation of the conformation tensor. Although we are able to prove theoretically energy dissipation of the scheme even for the diffusion coefficient $\varepsilon = 0$, our numerical experiments confirm more stable behaviour if $\varepsilon > 0$.

DOI: 10.1002/fld

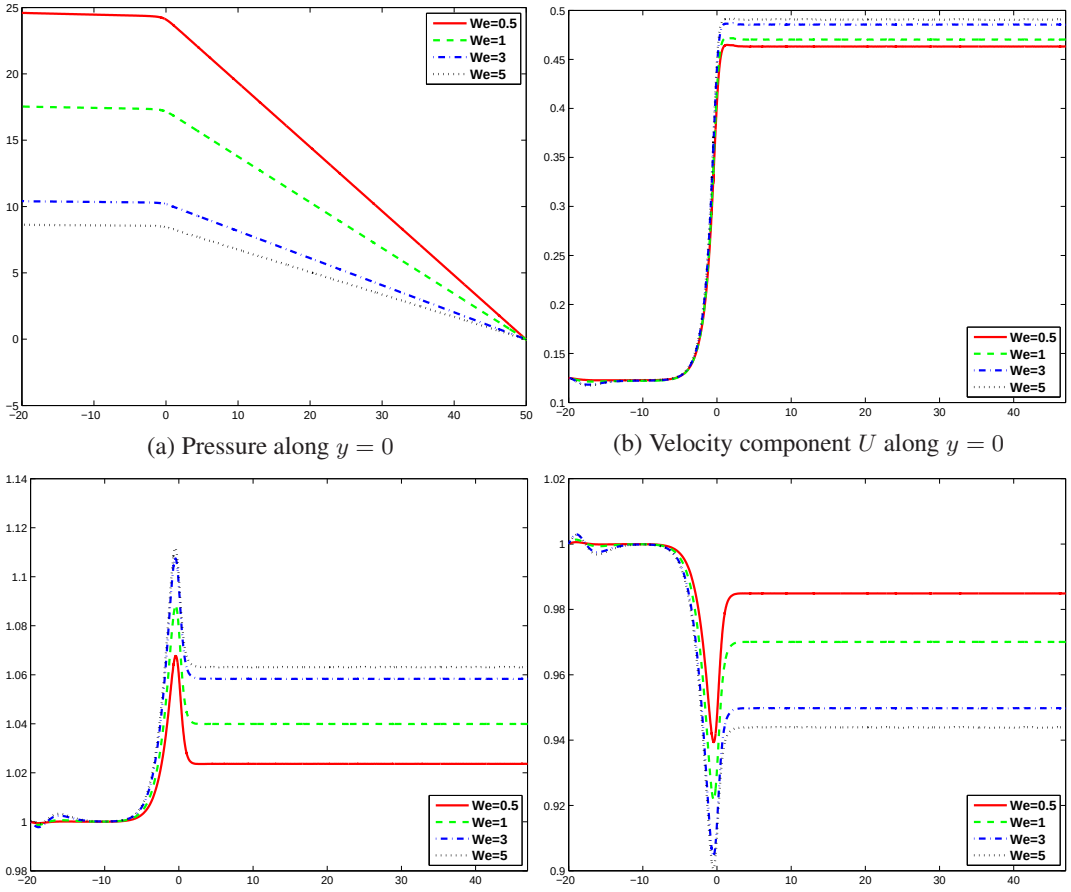

(a) Pressure along $y = 0$

(b) Velocity component U along $y = 0$

(c) σ_{11} along $y = 0$

(d) σ_{22} along $y = 0$

Figure 11. Results of the diffusive Oldroyd-B model, $\varepsilon = 1$, at $t = 1$ along the symmetric axis $y = 0$ for different We: pressure p, velocity component U, conformation components σ_{11} and σ_{22}, computed by the characteristic FEM, Algorithm 1.

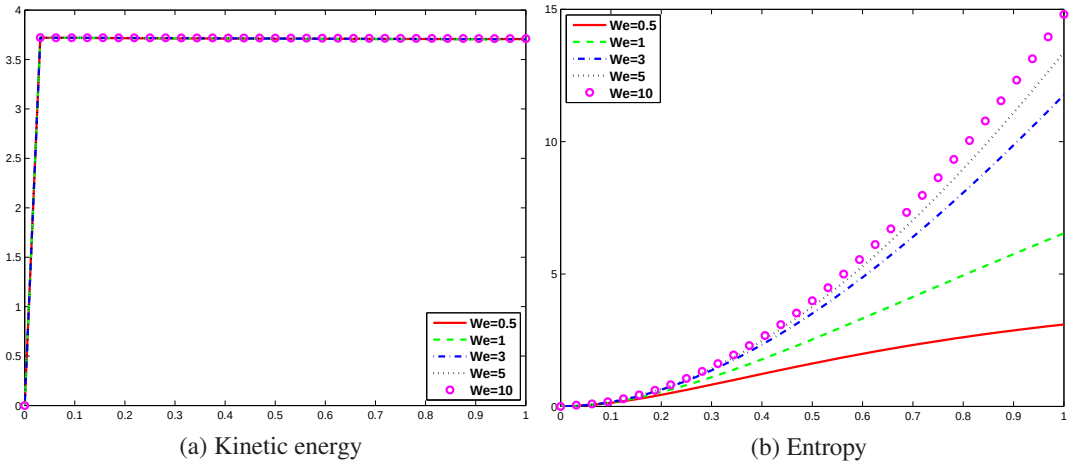

(a) Kinetic energy

(b) Entropy

Figure 12. Time evolution of the kinetic energy and entropy for the diffusive Oldroyd-B model with $\varepsilon = 0.01$ for different We, computed by the characteristic FEM, Algorithm 1.

DOI: 10.1002/fld

CONCLUSION

In this paper we have proposed and analyzed two energy stable numerical methods for the Oldroyd-B viscoelastic fluids. In particular, we have applied the logarithmic transformation for the conformation tensor including also diffusive effects in the equation of the conformation tensor. We have also shown that the new model dissipates the free energy, which is a sum of the kinetic energy and the entropy. For the numerical approximation we have studied the characteristic finite element and the characteristic finite difference methods. Moreover, we have shown that both the characteristic finite element and the finite difference schemes dissipate the free energy for arbitrary Weissenberg number.

In our numerical tests it has been observed that the diffusive models are more stable than the non-diffusive ones, in particular for high Weissenberg numbers. One important result, that we would like to emphasize is the fact that the mesh convergence has been obtained even for high Weissenberg numbers when using the diffusive Oldroyd-B model with the logarithmic transformation.

Acknowledgement. M.L-M. and B.S. were supported by the German Science Foundation under the grant IRTG 1529 "Mathematical Fluid Dynamics". H.N. was supported by JSPS (the Japan Society for the Promotion of Science) under the Japanese-German Graduate Externship "Mathematical Fluid Dynamics" and Grants-in-Aid for Young Scientists (B), No.26800091, and Scientific Research (S), No.24224004. We would like to thank Prof. Lelievre and Dr. Boyaval (Ecole des Ponts ParisTech, Paris) and Mizerova (University of Mainz) for fruitful discussions on the topic.

A. APPENDIX

A.1. Proof of Lemma 3

Proof

As $\boldsymbol{\sigma}$ and $\boldsymbol{\tau}$ are symmetric positive definite matrices, we have the following eigen-decomposition,

$$\boldsymbol{\sigma} = \mathbf{R}_1 \boldsymbol{\Lambda} \mathbf{R}_1^T, \quad \boldsymbol{\tau} = \mathbf{R}_2 \boldsymbol{\Gamma} \mathbf{R}_2^T,$$

where $\mathbf{R}_1$ and $\mathbf{R}_2$ are orthonormal eigenvector matrices, $\boldsymbol{\Lambda} = \text{diag}\{\lambda_i\}, \boldsymbol{\Gamma} = \text{diag}\{\gamma_i\}, i = 1, \cdots, d$, λ_i and γ_i are eigenvalues of $\boldsymbol{\sigma}$ and $\boldsymbol{\tau}$, respectively, and $d = 2, 3$ is the space dimension.

Let $\mathbf{O} = \mathbf{R}_2^T \mathbf{R}_1$, then $\mathbf{O}$ is also orthonormal.

$$\begin{aligned}
&\text{tr}\left(\boldsymbol{\sigma} f(\boldsymbol{\tau})\right) = \text{tr}\left(\mathbf{R}_1 \boldsymbol{\Lambda} \mathbf{R}_1^T \mathbf{R}_2 f(\boldsymbol{\Gamma}) \mathbf{R}_2^T\right) = \text{tr}\left(\mathbf{R}_2^T \mathbf{R}_1 \boldsymbol{\Lambda} \mathbf{R}_1^T \mathbf{R}_2 f(\boldsymbol{\Gamma})\right) = \text{tr}\left(\mathbf{O} \boldsymbol{\Lambda} \mathbf{O}^T f(\boldsymbol{\Gamma})\right) \\
&= \sum_{i,j} (\mathbf{O}\boldsymbol{\Lambda})_{ij} \left(\mathbf{O}^T f(\boldsymbol{\Gamma})\right)_{ji} = \sum_{i,j} \Big(\big(\sum_k \mathbf{O}_{ik} \Lambda_{kj} \big) \big(\sum_k \mathbf{O}_{kj} f(\Gamma)_{ki} \big) \Big) = \sum_{i,j} \Big(\big(\mathbf{O}_{ij} \Lambda_{jj} \big) \big(\mathbf{O}_{ij} f(\Gamma)_{ii} \big) \Big) \\
&= \sum_{i,j} \Big(\mathbf{O}_{ij}^2 \lambda_j f(\gamma_i) \Big).
\end{aligned}$$

Prepared using fldauth.cls
DOI: 10.1002/fld

Similarly, we have

$$\mathrm{tr}\,(\boldsymbol{\tau} f(\boldsymbol{\sigma})) = \sum_{i,j} \left(\mathbf{O}_{ij}^2 f(\lambda_j)\gamma_i\right).$$

Since $\mathbf{O}$ is orthonormal, $\sum_i \mathbf{O}_{ij}^2 = 1$ for any $j,\ j = 1, \cdots d$ and

$$\mathrm{tr}\,(\boldsymbol{\sigma} f(\boldsymbol{\sigma})) = \sum_j (\lambda_j f(\lambda_j)) = \sum_j \left(\lambda_j f(\lambda_j) \sum_i \mathbf{O}_{ij}^2\right).$$

Similarly, we have

$$\mathrm{tr}\,(\boldsymbol{\tau} f(\boldsymbol{\tau})) = \sum_i (\gamma_i f(\gamma_i)) = \sum_i \left(\gamma_i f(\gamma_i) \sum_j \mathbf{O}_{ij}^2\right).$$

Combining the above four equations we get

$$\begin{aligned}
&(\boldsymbol{\sigma} - \boldsymbol{\tau}) : \big(f(\boldsymbol{\sigma}) - f(\boldsymbol{\tau})\big) \\
&= \mathrm{tr}\Big((\boldsymbol{\sigma} - \boldsymbol{\tau}) \cdot \big(f(\boldsymbol{\sigma}) - f(\boldsymbol{\tau})\big)\Big) = \mathrm{tr}\big(\boldsymbol{\sigma} f(\boldsymbol{\sigma}) + \boldsymbol{\tau} f(\boldsymbol{\tau}) - \boldsymbol{\tau} f(\boldsymbol{\sigma}) - \boldsymbol{\sigma} f(\boldsymbol{\tau})\big) \\
&= \sum_j \left(\lambda_j f(\lambda_j) \sum_i \mathbf{O}_{ij}^2\right) + \sum_i \left(\gamma_i f(\gamma_i) \sum_j \mathbf{O}_{ij}^2\right) - \sum_{i,j} \left(\mathbf{O}_{ij}^2 f(\lambda_j)\gamma_i\right) - \sum_{i,j} \left(\mathbf{O}_{ij}^2 \lambda_j f(\gamma_i)\right) \\
&= \sum_j \lambda_j \sum_i \mathbf{O}_{ij}^2 \big(f(\lambda_j) - f(\gamma_i)\big) + \sum_i \gamma_i \sum_j \mathbf{O}_{ij}^2 \big(f(\gamma_i) - f(\lambda_j)\big) \\
&= \sum_{i,j} \mathbf{O}_{ij}^2 \big(f(\lambda_j) - f(\gamma_i)\big)(\lambda_j - \gamma_i).
\end{aligned}$$

If f is an increasing function, we get (12a)

$$(\boldsymbol{\sigma} - \boldsymbol{\tau}) : (f(\boldsymbol{\sigma}) - f(\boldsymbol{\tau})) \geq 0,$$

otherwise we get (12b)

$$(\boldsymbol{\sigma} - \boldsymbol{\tau}) : (f(\boldsymbol{\sigma}) - f(\boldsymbol{\tau})) \leq 0.$$

Furthermore, we obtain

$$\frac{\partial \boldsymbol{\sigma}}{\partial x} : \frac{\partial f(\boldsymbol{\sigma})}{\partial x} = \lim_{dx \to 0} \frac{\boldsymbol{\sigma}(x + dx) - \boldsymbol{\sigma}(x)}{dx} : \frac{f\left(\boldsymbol{\sigma}(x + dx)\right) - f\left(\boldsymbol{\sigma}(x)\right)}{dx}.$$

For $x > 0$ we know that $f(x) = \ln x$ is an increasing function, and $f(x) = \frac{1}{x}$ is a decreasing function. Using (12a) and (12b) we get

$$\frac{\partial \boldsymbol{\sigma}}{\partial x} : \frac{\partial (\ln \boldsymbol{\sigma})}{\partial x} \geq 0,\ \frac{\partial \boldsymbol{\sigma}}{\partial x} : \frac{\partial (\boldsymbol{\sigma}^{-1})}{\partial x} \leq 0.$$

Analogously, the above inequalities also hold for other space dimension. Thus we have

$$\nabla \boldsymbol{\sigma} : \nabla (\ln \boldsymbol{\sigma}) \geq 0,\ \nabla \boldsymbol{\sigma} : \nabla (\boldsymbol{\sigma}^{-1}) \leq 0,$$

DOI: 10.1002/fld

which concludes the proof. □

REFERENCES

1. M. ABOUBACAR, H. MATALLAH, AND M. F. WEBSTER, *Highly elastic solutions for Oldroyd-B and Phan-Thien/Tanner fluids with a finite volume/element method: planar contraction flows.*, J. Non-Newton. Fluid Mech., 103 (2002), pp. 65–103.
2. A. M. AFONSO, P. J. OLIVEIRA, F. T. PINHO, AND M. A. ALVES, *The log-conformation tensor approach in the finite-volume method framework.*, J. Non-Newton. Fluid Mech., 157 (2009), pp. 55–65.
3. A. M. AFONSO, F. T. PINHO, AND M. A. ALVES, *The kernel-conformation constitutive laws.*, J. Non-Newton. Fluid Mech., 167-168 (2012), pp. 30–37.
4. M. A. ALVES, P. J. OLIVEIRA, AND F. T. PINHO, *Benchmark solutions for the flow of Oldroyd-B and PTT fluids in planar contractions.*, J. Non-Newton. Fluid Mech., 110 (2003), pp. 45–75.
5. N. BALCI, B. THOMASES, M. RENARDY, AND C. R. DOERING, *Symmetric factorization of the conformation tensor in viscoelastic fluid models.*, J. Non-Newton. Fluid Mech., 166 (2011), pp. 546–553.
6. J. W. BARRETT AND S. BOYAVAL, *Existence and approximation of a (regularized) Oldroyd-B model.*, Math. Models Methods Appl. Sci., 21 (2011), pp. 1783–1837.
7. J. W. BARRETT AND E. SÜLI, *Existence of global weak solutions to some regularized kinetic models for dilute polymers.*, Multiscale Model. Simul., 6 (2007), pp. 506–546.
8. S. BOYAVAL, *Lid-driven-cavity simulations of Oldroyd-B models using free-energy-dissipative schemes*, in Numerical Mathematics and Advanced Applications 2009, G. Kreiss, P. Lötstedt, A. Målqvist, and M. Neytcheva, eds., Springer Berlin Heidelberg, 2010, pp. 191–198.
9. S. BOYAVAL, T. LELIÈVRE, AND C. MANGOUBI, *Free-energy-dissipative schemes for the Oldroyd-B model.*, ESAIM, Math. Model. Numer. Anal., 43 (2009), pp. 523–561.
10. X. CHEN, H. MARSCHALL, M. SCHÄFER, AND D. BOTHE, *A comparison of stabilisation approaches for finite-volume simulation of viscoelastic fluid flow*, Int. J. Comput. Fluid Dyn., 27 (2013), pp. 229–250.
11. A. J. CHORIN, *Numerical solution of the Navier-Stokes equations*, Math. Comp., 22 (1968), pp. 745–762.
12. P. G. CIARLET, *The Finite Element Method for Elliptic Problems.*, 1978.
13. P. CONSTANTIN AND M. KLIEGL, *Note on global regularity for two-dimensional Oldroyd-B fluids with diffusive stress.*, Arch. Ration. Mech. Anal., 206 (2012), pp. 725–740.
14. M. J. CROCHET, A. R. DAVIES, AND K. WALTERS, *Numerical Simulation of Non-Newtonian Flow.*, vol. 1 of Rheology Series, Elsevier, 1984.
15. M. J. CROCHET AND R. KEUNINGS, *Finite element analysis of die swell of a highly elastic fluid*, J. Non-Newton. Fluid Mech., 10 (1982), pp. 339–356.
16. H. DAMANIK, J. HRON, A. OUAZZI, AND S. TUREK, *A monolithic FEM approach for the log-conformation reformulation (LCR) of viscoelastic flow problems.*, J. Non-Newton. Fluid Mech., 165 (2010), pp. 1105–1113.
17. P. DEGOND AND H. LIU, *Kinetic models for polymers with inertial effects.*, Netw. Heterog. Media, 4 (2009), pp. 625–647.
18. S. S. EDUSSURIYA, A. J. WILLIAMS, AND C. BAILEY, *A cell-centred finite volume method for modelling viscoelastic flow.*, J. Non-Newton. Fluid Mech., 117 (2004), pp. 47–61.
19. R. FATTAL AND R. KUPFERMAN, *Constitutive laws for the matrix-logarithm of the conformation tensor.*, J. Non-Newton. Fluid Mech., 123 (2004), pp. 281–285.
20. ———, *Time-dependent simulation of viscoelastic flows at high Weissenberg number using the log-conformation representation.*, J. Non-Newton. Fluid Mech., 126 (2005), pp. 23–37.
21. R. GUNETTE AND M. FORTIN, *A new mixed finite element method for computing viscoelastic flows.*, J. Non-Newton. Fluid Mech., 60 (1995), pp. 27–52.
22. J. HAO AND T. PAN, *Simulation for high Weissenberg number: Viscoelastic flow by a finite element method.*, Appl. Math. Lett., 20 (2007), pp. 988–993.
23. D. HU AND T. LELIÈVRE, *New entropy estimates for the Oldroyd-B model and related models.*, Commun. Math. Sci., 5 (2007), pp. 909–916.
24. M. A. HULSEN, R. FATTAL, AND R. KUPFERMAN, *Flow of viscoelastic fluids past a cylinder at high Weissenberg number: stabilized simulations using matrix logarithms.*, J. Non-Newton. Fluid Mech., 127 (2005), pp. 27–39.
25. R. KEUNINGS, *On the high weissenberg number problem*, J. Non-Newton. Fluid Mech., 20 (1986), pp. 209–226.

DOI: 10.1002/fld

26. ———, *A survey of computational rheology*, Proceedings of the XIIIth International Congress on Rheology, 1 (2000), pp. 7–14.
27. A. LE HYARIC, *An Integrated Environment for FreeFem++*.
28. Y. LEE AND J. XU, *New formulations, positivity preserving discretizations and stability analysis for non-Newtonian flow models.*, Comput. Meth. Appl. Mech. Eng., 195 (2006), pp. 1180–1206.
29. Y. LEE, J. XU, AND C. ZHANG, *Stable finite element discretizations for viscoelastic flow models*, in Numerical Methods for Non-Newtonian Fluids, R. Glowinski and J. Xu, eds., vol. 16 of Handbook of Numerical Analysis, Elsevier, 2011, pp. 371–432.
30. J. LI AND S. SUN, *The superconvergence phenomenon and proof of the MAC scheme for the Stokes equations on non-uniform rectangular meshes*, J. Sci. Comput, DOI 10.1007/s10915-014-9963-5, (2014).
31. M. LUKÁČOVÁ, H. MIZEROVÁ, B. SHE, AND J. STEBEL, *Error analysis of the finite element and finite volume methods for some viscoelastic fluids.* accepted to J. Num. Math., 2015.
32. J. M. MARCHAL AND M. J. CROCHET, *A new mixed finite element for calculating viscoelastic flow*, J. Non-Newton. Fluid Mech., 26 (1987), pp. 77–114.
33. L. NADAU AND A. SEQUEIRA, *Numerical simulations of shear-dependent viscoelastic flows with a combined finite element-finite volume method.*, Comput. Math. Appl., 53 (2007), pp. 547–568.
34. H. NOTSU AND M. TABATA, *Error estimates of a pressure-stabilized characteristics finite element scheme for the Oseen equations.*, J. Sci. Comput., (2015), pp. 1–16.
35. ———, *Error estimates of a stabilized Lagrange-Galerkin scheme for the Navier-Stokes equations.*, to appear in ESAIM, Math. Model. Numer. Anal., (2015).
36. T. PAN AND J. HAO, *Numerical simulation of a lid-driven cavity viscoelastic flow at high Weissenberg numbers.*, C. R., Math., Acad. Sci. Paris, 344 (2007), pp. 283–286.
37. T. N. PHILLIPS AND A. J. WILLIAMS, *Viscoelastic flow through a planar contraction using a semi-lagrangian finite volume method*, J. Non-Newton. Fluid Mech., 87 (1999), pp. 215–246.
38. O. PIRONNEAU, *On the transport-diffusion algorithm and its applications to the Navier-Stokes equations.*, Numer. Math., 38 (1982), pp. 309–332.
39. J. D. SCHIEBER, *Generalized Brownian configuration fields for Fokker-Planck equations including center-of-mass diffusion.*, J. Non-Newton. Fluid Mech., 135 (2006), pp. 179–181.
40. B. SEIBOLD, *A compact and fast Matlab code solving the incompressible Navier-Stokes equations on rectangular domains.* University Lecture, available at http://math.mit.edu/classes/18.086/2008/, 2008.
41. B. SHE, *Numerical Simulation of Some Viscoelastic Fluids.*, PhD thesis, Johannes Gutenberg-Universität Mainz, 2015.
42. D. TREBOTICH, P. COLELLA, AND G. H. MILLER, *A stable and convergent scheme for viscoelastic flow in contraction channels*, J. Comput. Phys., 205 (2005), pp. 315–342.
43. K. WALTERS AND M. F. WEBSTER, *The distinctive CFD challenges of computational rheology.*, Int. J. Numer. Methods Fluids, 43 (2003), pp. 577–596.
44. P. WAPPEROM, R. KEUNINGS, AND V. LEGAT, *The backward-tracking lagrangian particle method for transient viscoelastic flows*, J. Non-Newton. Fluid Mech., 91 (2000), pp. 273–295.
45. P. WAPPEROM AND M. F. WEBSTER, *Simulation for viscoelastic flow by a finite volume/element method*, Comput. Meth. Appl. Mech. Eng., 180 (1999), pp. 281–304.
46. S.-C. XUE, N. PHAN-THIEN, AND R. I. TANNER, *Three dimensional numerical simulations of viscoelastic flows through planar contractions*, J. Non-Newton. Fluid Mech., 74 (1998), pp. 195–245.

DOI: 10.1002/fld

Table I. Error norms and EOC for diffusive Oldroyd-B model (8), $\varepsilon = 0.01$, computed by the characteristic FEM, Algorithm 1.

h	$e(\mathbf{u}_h)$	$e(p_h)$	$e(\boldsymbol{\sigma}_h)$	$e_1(\mathbf{u}_h)$	$e_1(p_h)$	$e_1(\boldsymbol{\sigma}_h)$
1/8	1.77×10^{-2}	2.11×10^{-1}	4.46×10^{-1}	6.24×10^{-1}	6.97×10^{-1}	6.33×10^{0}
1/16	5.32×10^{-3}	5.88×10^{-2}	1.04×10^{-1}	3.45×10^{-1}	2.32×10^{-1}	3.35×10^{0}
1/32	1.23×10^{-3}	2.36×10^{-2}	2.87×10^{-2}	1.64×10^{-1}	8.74×10^{-2}	1.69×10^{0}
1/64	3.41×10^{-4}	8.77×10^{-3}	8.57×10^{-3}	8.05×10^{-2}	3.90×10^{-2}	8.39×10^{-1}
			EOC			
1/8	1.73	1.84	2.10	0.85	1.58	0.92
1/16	2.12	1.32	1.85	1.07	1.41	0.99
1/32	1.85	1.43	1.74	1.03	1.17	1.01

(a) We=0.5

h	$e(\mathbf{u}_h)$	$e(p_h)$	$e(\boldsymbol{\sigma}_h)$	$e_1(\mathbf{u}_h)$	$e_1(p_h)$	$e_1(\boldsymbol{\sigma}_h)$
1/8	1.84×10^{-2}	2.42×10^{-1}	1.05×10^{0}	6.33×10^{-1}	7.55×10^{-1}	1.45×10^{1}
1/16	5.41×10^{-3}	6.74×10^{-2}	2.29×10^{-1}	3.49×10^{-1}	2.35×10^{-1}	6.64×10^{0}
1/32	1.26×10^{-3}	2.63×10^{-2}	6.14×10^{-2}	1.65×10^{-1}	8.91×10^{-2}	3.17×10^{0}
1/64	3.40×10^{-4}	1.06×10^{-2}	2.19×10^{-2}	8.14×10^{-2}	3.97×10^{-2}	1.60×10^{0}
			EOC			
1/8	1.76	1.84	2.20	0.86	1.68	1.13
1/16	2.10	1.36	1.90	1.08	1.40	1.07
1/32	1.89	1.32	1.48	1.02	1.17	0.99

(b) We=1

h	$e(\mathbf{u}_h)$	$e(p_h)$	$e(\boldsymbol{\sigma}_h)$	$e_1(\mathbf{u}_h)$	$e_1(p_h)$	$e_1(\boldsymbol{\sigma}_h)$
1/8	1.56×10^{-2}	1.84×10^{-1}	2.12×10^{0}	5.85×10^{-1}	5.55×10^{-1}	3.15×10^{1}
1/16	4.69×10^{-3}	9.74×10^{-2}	1.06×10^{0}	3.19×10^{-1}	2.19×10^{-1}	1.86×10^{1}
1/32	1.08×10^{-3}	3.07×10^{-2}	3.27×10^{-1}	1.51×10^{-1}	8.18×10^{-2}	8.05×10^{0}
1/64	3.16×10^{-4}	1.21×10^{-2}	1.31×10^{-1}	7.54×10^{-2}	3.68×10^{-2}	4.12×10^{0}
			EOC			
1/8	1.73	0.91	0.99	0.88	1.34	0.76
1/16	2.11	1.67	1.70	1.07	1.42	1.21
1/32	1.78	1.34	1.32	1.01	1.15	0.97

(c) We=5

h	$e(\mathbf{u}_h)$	$e(p_h)$	$e(\boldsymbol{\sigma}_h)$	$e_1(\mathbf{u}_h)$	$e_1(p_h)$	$e_1(\boldsymbol{\sigma}_h)$
1/8	1.37×10^{-2}	1.16×10^{-1}	3.21×10^{0}	5.52×10^{-1}	4.33×10^{-1}	3.54×10^{1}
1/16	3.93×10^{-3}	4.99×10^{-2}	1.23×10^{0}	2.99×10^{-1}	1.88×10^{-1}	2.09×10^{1}
1/32	8.03×10^{-4}	1.70×10^{-2}	3.38×10^{-1}	1.39×10^{-1}	7.47×10^{-2}	8.40×10^{0}
1/64	1.97×10^{-4}	7.01×10^{-3}	9.71×10^{-2}	7.29×10^{-2}	3.54×10^{-2}	4.23×10^{0}
			EOC			
1/8	1.80	1.22	1.38	0.88	1.21	0.76
1/16	2.29	1.55	1.86	1.10	1.33	1.31
1/32	2.02	1.28	1.80	0.93	1.07	0.99

(d) We=50

DOI: 10.1002/fld

Table II. Error norms and EOC for diffusive Oldroyd-B model (8), $\varepsilon = 0.01$, computed by the characteristic finite difference method, Algorithm 2.

h	$e(\mathbf{u}_h)$	$e(p_h)$	$e(\boldsymbol{\sigma}_h)$	$e_1(\mathbf{u}_h)$	$e_1(p_h)$	$e_1(\boldsymbol{\sigma}_h)$
1/8	2.12×10^{-2}	6.24×10^{-1}	5.61×10^{-1}	2.23×10^{-1}	4.83×10^{0}	7.03×10^{0}
1/16	6.81×10^{-3}	2.80×10^{-1}	3.01×10^{-1}	8.75×10^{-2}	2.58×10^{0}	4.11×10^{0}
1/32	1.99×10^{-3}	1.12×10^{-1}	1.37×10^{-1}	3.24×10^{-2}	1.17×10^{0}	1.73×10^{0}
1/64	6.05×10^{-4}	3.57×10^{-2}	4.70×10^{-2}	1.02×10^{-2}	3.77×10^{-1}	5.55×10^{-1}
			EOC			
1/8	1.64	1.15	0.90	1.35	0.90	0.78
1/16	1.78	1.32	1.14	1.43	1.15	1.25
1/32	1.72	1.65	1.54	1.67	1.63	1.64

(a) We=0.5

h	$e(\mathbf{u}_h)$	$e(p_h)$	$e(\boldsymbol{\sigma}_h)$	$e_1(\mathbf{u}_h)$	$e_1(p_h)$	$e_1(\boldsymbol{\sigma}_h)$
1/8	2.07×10^{-2}	6.28×10^{-1}	1.23×10^{0}	2.41×10^{-1}	4.82×10^{0}	1.32×10^{1}
1/16	7.26×10^{-3}	2.95×10^{-1}	6.70×10^{-1}	1.05×10^{-1}	2.64×10^{0}	8.03×10^{0}
1/32	2.68×10^{-3}	1.25×10^{-1}	3.12×10^{-1}	4.28×10^{-2}	1.24×10^{0}	3.51×10^{0}
1/64	9.43×10^{-4}	4.18×10^{-2}	1.10×10^{-1}	1.42×10^{-2}	4.13×10^{-1}	1.17×10^{0}
			EOC			
1/8	1.51	1.09	0.87	1.21	0.87	0.72
1/16	1.44	1.24	1.10	1.29	1.09	1.19
1/32	1.51	1.58	1.51	1.59	1.59	1.58

(b) We=1

h	$e(\mathbf{u}_h)$	$e(p_h)$	$e(\boldsymbol{\sigma}_h)$	$e_1(\mathbf{u}_h)$	$e_1(p_h)$	$e_1(\boldsymbol{\sigma}_h)$
1/8	2.08×10^{-2}	3.76×10^{-1}	3.32×10^{0}	2.26×10^{-1}	3.08×10^{0}	3.42×10^{1}
1/16	6.99×10^{-3}	1.89×10^{-1}	2.01×10^{0}	9.11×10^{-2}	1.70×10^{0}	2.13×10^{1}
1/32	2.84×10^{-3}	8.78×10^{-2}	1.03×10^{0}	3.80×10^{-2}	8.29×10^{-1}	1.02×10^{1}
1/64	1.10×10^{-3}	3.16×10^{-2}	3.90×10^{-1}	1.35×10^{-2}	2.78×10^{-1}	3.71×10^{0}
			EOC			
1/8	1.58	0.99	0.72	1.31	0.86	0.68
1/16	1.30	1.11	0.97	1.26	1.03	1.06
1/32	1.37	1.47	1.40	1.49	1.57	1.46

(c) We=5

h	$e(\mathbf{u}_h)$	$e(p_h)$	$e(\boldsymbol{\sigma}_h)$	$e_1(\mathbf{u}_h)$	$e_1(p_h)$	$e_1(\boldsymbol{\sigma}_h)$
1/8	1.99×10^{-2}	1.51×10^{-1}	3.42×10^{0}	1.94×10^{-1}	1.62×10^{0}	3.51×10^{1}
1/16	5.89×10^{-3}	4.73×10^{-2}	2.10×10^{0}	6.00×10^{-2}	6.78×10^{-1}	2.11×10^{1}
1/32	1.43×10^{-3}	1.48×10^{-2}	1.12×10^{0}	1.59×10^{-2}	2.22×10^{-1}	1.05×10^{1}
1/64	2.81×10^{-4}	4.34×10^{-3}	4.33×10^{-1}	3.59×10^{-3}	5.18×10^{-2}	3.93×10^{0}
			EOC			
1/8	1.76	1.68	0.70	1.70	1.25	0.73
1/16	2.04	1.68	0.91	1.92	1.61	1.02
1/32	2.35	1.77	1.37	2.14	2.10	1.41

(d) We=50

DOI: 10.1002/fld

Table III. Error norms and EOC for diffusive Oldroyd-B model (8), $\varepsilon = 0.01$, computed by the characteristic finite difference method, with characteristic discretization also in the Navier-Stokes part.

h	$e(\mathbf{u}_h)$	$e(p_h)$	$e(\boldsymbol{\sigma}_h)$	$e_1(\mathbf{u}_h)$	$e_1(p_h)$	$e_1(\boldsymbol{\sigma}_h)$
1/8	2.74×10^{-2}	3.16×10^{-1}	7.57×10^{-1}	2.28×10^{-1}	3.05×10^{0}	1.07×10^{1}
1/16	8.05×10^{-3}	8.17×10^{-2}	2.38×10^{-1}	7.57×10^{-2}	1.18×10^{0}	5.60×10^{0}
1/32	1.90×10^{-3}	2.15×10^{-2}	7.47×10^{-2}	2.20×10^{-2}	3.89×10^{-1}	1.92×10^{0}
1/64	3.82×10^{-4}	5.65×10^{-3}	2.28×10^{-2}	5.72×10^{-3}	9.90×10^{-2}	5.72×10^{-1}
			EOC			
1/8	1.76	1.95	1.67	1.59	1.37	0.94
1/16	2.08	1.92	1.67	1.78	1.60	1.55
1/32	2.32	1.93	1.71	1.95	1.97	1.75

DOI: 10.1002/fld